07/30/2012
TD-12-11

Study of Superconducting-to-Resistive Transition for the US-LARP Large High Field Quadrupoles for the LHC Upgrade

Lidia Rossi

Abstract

The goal of this thesis, in the context of the *High Luminosity LHC* project, is the improvement of quench simulation through comparisons with experimental data. This study is based on comparisons between simulations and experimental data collected during the test of LARP LQS01b quadrupole magnet. Simulations were mostly made by means of the computer code QuenchPro, developed at FNAL. In the final part of this study we also used QLASA, a computer code for quench simulation in adiabatic multicoil superconducting windings developed at INFN-LASA (Milan, Italy).
After an introduction to superconducting magnets and in particular to the Long Nb_3Sn Quadrupole (LQS01b) the computer codes and the experiments are described in details.
The last chapter reports the data analysis with the most interesting studies that have led to a better understanding of the LQS01b quench behavior. The modifications to QuenchPro introduced in order to get more realistic simulations of the quench in Nb_3Sn accelerator magnets are also reported.

"It has nothing to do directly with defending our country except to make it worth defending"
Robert Wilson
Congressional Join Committee on Atomic Energy, April 1969

To my grandmother and my parents

Contents

Introduction **5**

1 Stability of superconducting magnets and causes of degradation **7**
1.1 Introduction . . . 7
1.2 Degradation and training . . . 9
1.2.1 The disturbance spectrum . . . 9
1.2.2 Quench performance of a magnet . . . 11
1.2.3 Distributed disturbances . . . 11
1.2.4 Point disturbances . . . 13
1.2.4.1 A wire purely of superconductor . . . 13
1.2.4.2 Stabilization: superconductor surrounded by a metal . . . 14
1.2.5 Minimum propagating zone . . . 15
1.3 Quenching and protection . . . 16
1.3.1 Quench consequences . . . 16
1.3.1.1 Temperature rise . . . 16
1.3.1.2 Voltage distribution . . . 17
1.3.2 Quench propagation velocity . . . 18
1.3.2.1 Longitudinal propagation velocity . . . 18
1.3.2.2 Transverse propagation velocity . . . 19
1.3.3 Protection methods . . . 19
1.3.3.1 External dump resistor . . . 20
1.3.3.2 Induction of coupled secondary circuit (s) . . . 20
1.3.3.3 Active protection using heaters . . . 21

2 LARP Long Nb_3Sn Quadrupole Design **23**
2.1 Introduction . . . 23
2.2 Nb_3Sn Superconducting Magnets for Particle Accelerators . . . 24
2.2.1 Superconducting magnets for particle accelerators . . . 24
2.2.2 Basic properties of Nb_3Sn . . . 25
2.2.2.1 Multifilament wires: Motivations and Fabrication . . . 25
2.2.2.2 Superconducting cables . . . 30
2.3 The Long Quadrupole . . . 32
2.3.1 Magnet Design . . . 32
2.3.2 Coil design and fabrication . . . 34
2.3.3 Mechanical design . . . 35

3 Quench Protection of the Long Quadrupole **37**
3.1 Introduction . . . 37
3.2 Quench Protection . . . 37
3.2.1 Protection design . . . 37
3.2.2 LQS01b Instrumentation . . . 37
3.2.3 Protection heaters . . . 38
3.2.4 Protection with dump resistor . . . 39
3.3 Quench History . . . 40
3.4 Quench simulations: QuenchPro . . . 41
3.4.1 Input Parameters . . . 43
3.4.1.1 Material Properties . . . 43
3.4.1.2 Magnet operational parameters . . . 43
3.4.1.3 Quench Protection System Parameters . . . 43
3.4.2 Output Parameters . . . 43
3.4.3 Program lay-out . . . 44
3.5 Quench simulation: QLASA . . . 46

4 The experiment **51**
4.1 Introduction . . . 51
4.2 Test facility for superconducting accelerator magnets . . . 51
4.2.1 Test facility . . . 51
4.2.2 Quench test procedure . . . 56

5 Data analysis **59**
5.1 First comparisons between experimental and simulation data . . . 59
5.2 Second part of the study . . . 64
5.2.1 Study of the 1st area . . . 65
5.2.1.1 Experimental data . . . 65
5.2.1.2 Study of the dynamic inductance from the computation of the energy 66
5.2.1.3 Measurements of the inductance at room temperature . . . 67
5.2.1.4 Conclusion of the study of the dynamic inductance . . . 68
5.2.1.5 Measurements of the effect of the eddy currents on L . . . 69
5.2.1.6 Comparison of simulated current decay and experimental . . . 69
5.2.2 Study of the 2nd area . . . 71
5.2.3 Finals comparisons between experimental data, QuenchPro and QLASA . . . 73
5.2.3.1 QLASA velocities . . . 73
5.2.3.2 Comparisons . . . 73

Conclusions **77**

Appendix: Energy computed by OPERA **79**

Acknowledgments **81**

Bibliography **83**

Introduction

In this thesis we study the behavior of superconducting magnets based on Nb_3Sn conductor, specifically when they operate near to the critical values of field and current.

In particular, we investigate the modality of propagation of a region that underwent a transition from superconducting state to resistive state; this phenomenon is called QUENCH.

These studies are very interesting and fundamental for the design of advanced accelerator magnets, because of their very high current density. Despite the fact that the magnets are equipped with important and sophisticated safety systems, avoiding serious damage to the magnets (especially when operating near their maximum performance), the protection is a very challenging issue.

In this thesis, carried out at Fermilab in the Techinical Division, we study a quadrupole, named LQS01b, which is the first prototype for the project "High Luminosity LHC" which aims to upgrade the LHC accelerator at CERN in Geneva (Switzerland). Fermilab is carrying out this research in collaboration with other laboratories in the US through LARP (LHC Accelerator Research Program).

The goal of this study is to compare experimental data and simulations carried out with numerical codes, in order to understand the behavior of the magnet and to improve the simulation codes for future magnets. For the simulations we used two different programs: QuenchPro and QLASA. The first program, which is the principal program that we have used during the work at Fermilab, was written specifically for this kind of superconducting magnet, while the second was intended for a superconducting solenoid. We used these programs to study the current decay in presence of a quench.

In Chapter 1 we will describe the stability of superconducting magnets and the causes of degradation and training. This chapter contains a discussion of theoretical applied superconductivity.

In Chapter 2, after a short introduction to accelerator magnets and the Nb_3Sn superconductor, we will describethe Long Nb_3Sn Quadrupole LQS01b.

In Chapter 3 we will describe the quench protection provided by, the Long Quadrupole. We will also describe, QuenchPro and QLASA.

In Chapter 4 we will describe the experiment, i.e., the test facility for superconducting magnets and the quench test procedure.

In Chapter 5 we will analyze the data, comparing the QuenchPro and QLASA simulations. The adaptation of the two codes in order to achieve satisfactory results will also be discussed, together with the overall results of the thesis.

Chapter 1

Stability of superconducting magnets and causes of degradation

1.1 Introduction

[1]Superconductivity is the name given to a remarkable phenomenon, discovered by Kammerlingh Onnes in 1911, whereby certain metals when cooled to very low temperatures below the critical temperature T_c (a characteristic of each metal) become perfect conductors of electricity, i.e. the resistance is absolutely zero. To describe this property it is necessary to introduce the concepts of critical temperature T_c to those the critical field B_c and current density J_c. These parameters are inter-related, and in the space T-B-J they define a surface, called critical surface. A section of the critical surface at constant T, for example, give the curve $J_c = J_c(B)$ etc..The critical surface in the space T-B-J of $G_c\ (T, B, J) = 0$ is the separation between the normal resistivity phase and the superconducting phase. An increase in any one of the properties invariably produces a decrease in the other two. A superconducting magnet works in the superconductivity phase: $G\ (T, B, J) \leq G_c\ (T, B, J)$. The superconductors discovered by Onnes are today called types-I superconductors and they are known for having a very small critical field (0.01-0.1 T) and current density $(1 - 10\ A/mm^2)$.

[1]This Chapter refers to [1]

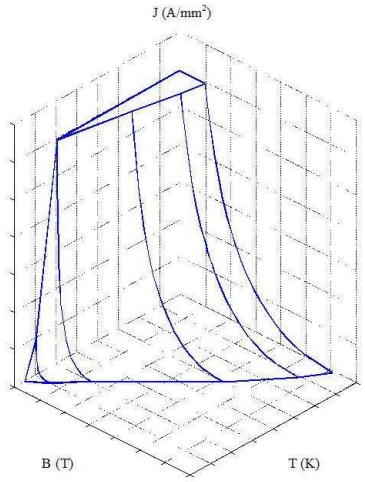

Figure 1.1: Critical surface for Nb_3Sn [2]

At the beginning of 1960, in USA, a new class of high-field superconducting alloy was discovered: type-II superconductors. These materials are able to withstand very high fields and to carry extremely high-current. The most popular superconducting alloys are Niobium Titanium NbTi) and Niobium Tin (Nb_3Sn) (the latter which has much better performance but is more difficult to work with because it is weak and brittle). The usual operating temperature for superconducting magnets is T= 4.2 K because is the boiling point of liquid helium under atmospheric pressure. Anohter possible choice for the temperature is around 2 K, which is the temperature of superfluid helium (used for the LHC magnets). In conclusion, once materials with usable superconducting properties are known it is possible to use them to design magnets with the desired characteristics and performances, in terms of magnetic field, dimensions, and current density. But normally is very difficult to get the current maximum values theoretically expected, given by their Current Limit, CL indicated in the figure below.

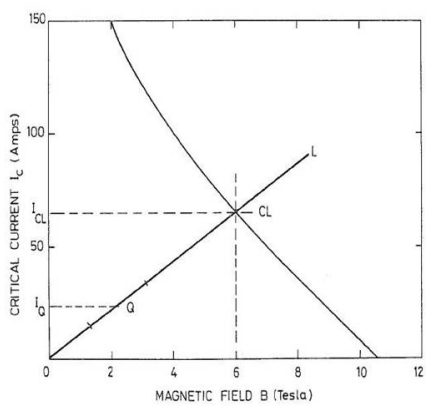

Figure 1.2: Short-sample critical current I_c for NbTi and load line for a small solenoid

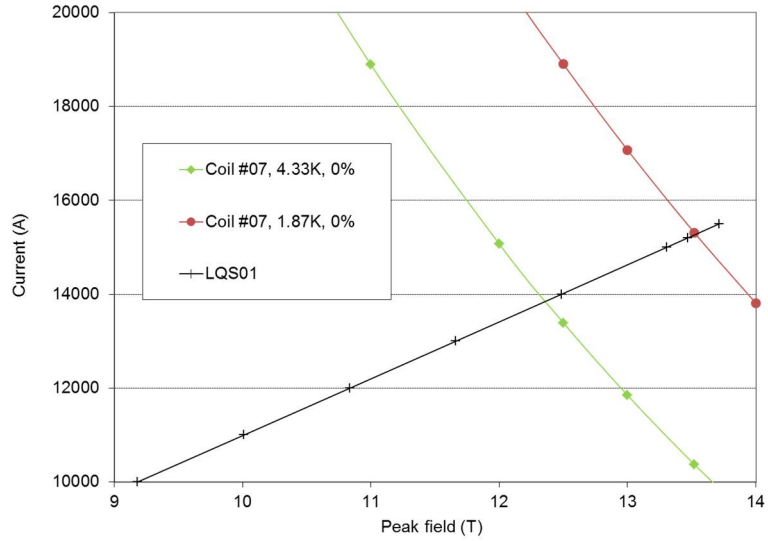

Figure 1.3: Short-sample critical current I_c for Nb_3Sn and load line for LQS01b

In practice it is found that the magnets goes from a superconducting to a normal resistive state well before reaching the maximum theoretical current. Because normal-state resistivities and current densities are both high, intense local heating will follow, taking the quench point and surrounding region to temperatures far above critical. This phenomenon is an irreversible process causing the entire stored energy $\frac{1}{2}LI^2$ of the magnet to be dissipated as heat.

Restoring a magnet's operating condition takes a few minutes for laboratory size systems, or days for larger systems. Because of the high current and high stored energies in these magnets, the quench process can produce violent effects.

Once the magnet is energized, again, usually the new level of current at which it will quench is higher than the one of the previous energization. This progressive improvement in current towards the theoretical maximum is called "Training". A good magnet has fast training, reaching the maximum with a few cycles of cool-down, energization and warm-up. Lower qualisty magnets may require 20-30 quenches or more. It may happen that the magnet never reaches its theoretical maximum of current: this phenomenon is called "Degradation". Degradation may be a problem if it is more than 10% (taking into account that the theoretical maximum is not always precisely known). In general both degradation and training varies with the conductor used, the coil shape, and the method of construction.

1.2 Degradation and training

1.2.1 The disturbance spectrum

The origin of a degradation might be a weak spot somewhere along the wire, which is many kilometres long, even in magnets of modest size, but the problem is usually caused by the release of energy inside the magnet as the current and field are increased. Temperatures rise locally, which could lead to a transition in a limited zone, affecting the entire magnet at transition.

We can define a spectrum of energy disturbances, according to two dimensions: time and space.

Table 1.1: The disturbace spectrum

		Space	
		Point	Distributed
Time	Transient	J	J/m^3
	Continuous	W	W/m^3

Continuous disturbances are due to steady power dissipation in the coil. These disturbances are usually quite regular and reproducible; they will not produce training, although they may produce considerable degradation. They are usually well understood disturbances. These include:

- A bad joint between two lengths of conductor
- Excessive a.c. losses in the conductor, caused by the slight resistance which is developed in conductors as they approach critical current, by mechanical hysteresis effects, or by an extraneous heat leak coming from a faulty cryogenic system.

Transient disturbances are a much more serious problem; they are thought to be the dominant cause of degradation and training in present-day magnets. Transient quenches are due to a sudden release of energy, either over a small volume (J) or over a large volume (J/m^3).

- Flux jumps: dissipative redistribution of magnetic field within the superconductor. These can be eliminated (with NbTi wire) or reduced (with Nb_3Sn) with small filaments. Our wires are sufficiently high in current density that flux jumps are never fully eliminated, and in some cases the basic e.m. instability may play an important role.
- Mechanical disturbances: wire frictional motion and epoxy cracking. These are less predictable and are difficult to avoid because they are related to mechanical design, material properties, fabrication processes, etc. For example, if we indicate with S a displacement of a coil in the field B, the work W of the forces that are dissipated in a heat pulse is: W= BJS. We have high magnetic field and high currents (this characterizes the superconducting regime) so a minimum displacement (e.g., one micrometer) can induce a quench. To avoid these problems the magnets are impregnated with appropriate resins in order to immobilize the coils of the winding. This solution solves the problem discussed above; however, it produces other problems during the excitation of the coils, the resins, which are not very elastic at very low temperatures, are subject to micro-fractures which release heat.

In a case of quench, a magnet which completely impregnated, cooled only to the external walls of the winding, dissipates all the magnetic energy inside the magnet, due to its low thermal conductivity; thus the quench propagates and evolves with almost no energy exchanged toward the external bath. For this reason we call this kind of magnets an adiabatic magnets. Alternatively magnets which are directly immersed in cryogenic liquid and with considerable exchange surface are called cryogenically stabilize magnets.

We are most interested in adiabatic magnets because it is necessary to impregnate the Nb_3Sn coils after heat treatment.

1.2.2 Quench performance of a magnet

A quench is usually generated by small energy release due to flux jump and more frequently to motion and friction of small part of the superconductor. Under e.m. force the conductor is put in position more stable, so the new ramp will activated a motion of a conductor region that was more stable than the previous one. This increase of the quench level with the ramp number is called "Training". The training ends when the increase of quench current, and therefore quench field, flattens out. If this flat top value is equal to the maximum quench current, i.e. the intersection of the load line with the critical current, the magnets is very good. If the flat top value is less, the magnet is "degradaded". Ideally magnet shoud have short training, i.e. reaching the flat top in 2-5 quenches and have little degradation (for Nb_3Sn accelerator magnets a degradation not more of 10% is good). If the magnet si strongly degrade, usually is limited by mechanics, i.e. the structure can't to keep the e.m. forces. Another important parameters is the memory. After the magnet has reached the flat top, one performs a full warm up of the magnet at room temperature, and then is cooled down again and a new training cycle starts. If the magnets starts training at the same level as it started at the previous thermal cycle, it means that the magents re-trains. If the magnet restart form the previous flat top, it means that it has a full memory of the previous thermal cycle. Often, our magnets have an intermediate behavior with a partial memory. Memory is one of the most important characteristics of accelerators magnets.

In Figure 1.4 is reported an example of a quench performance of a magnet:

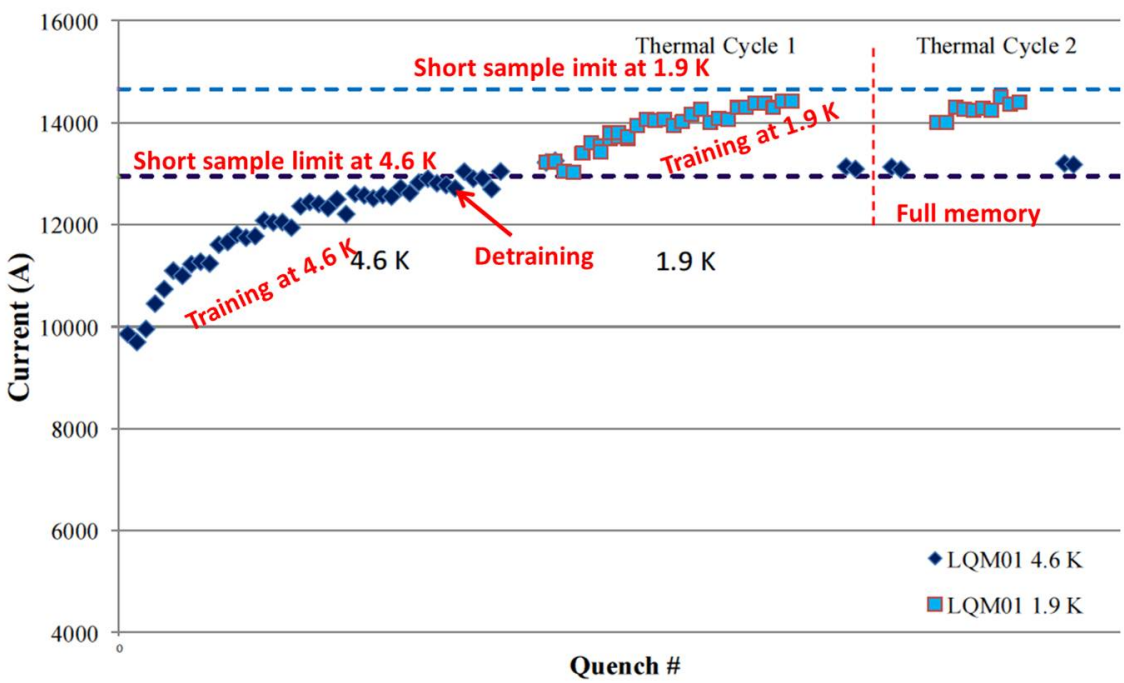

Figure 1.4: LQM01 training

1.2.3 Distributed disturbances

If we study the dependence of critical current density as a function of temperature at different critical field values, we can observe that this falls more or less linearly, at least for temperatures above 4.2K and reaching zero at a critical temperature T_c which is a decreasing function of magnetic field.

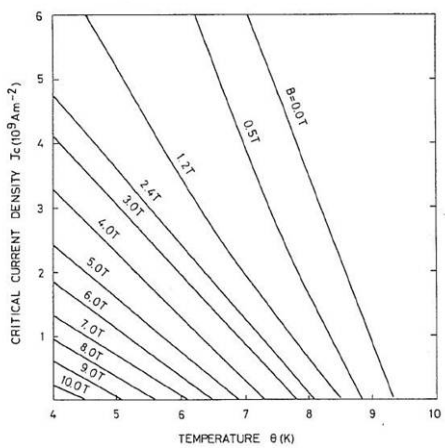

Figure 1.5: Temperature dependence of critical density in Niobium Titanium

Because J_c always falls with temperature, a magnet operating very near its critical current will be driven into the normal state by the slightest increase in temperature. A margin of security can be provided by running the magnet at subcritical current; if transient disturbances are present in the magnet and if they are sufficiently small, the magnet will only reach some fraction of its critical current, without contacting the critical surface. Figure 1.6 illustrates how, in a conductor which is carrying current density J_m, ohmic heat generation will begin when the temperature has risen to T_{cs}.

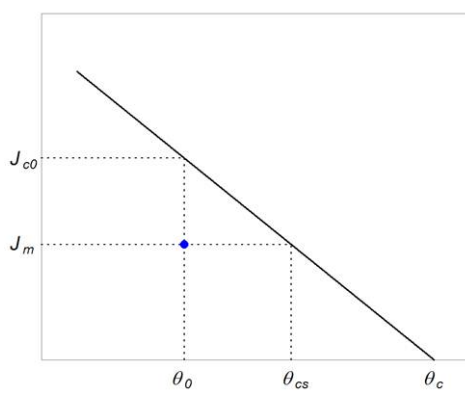

Figure 1.6: Critical current density as a function of temperature showing the temperature T_{cs}at which ohmic heat generation starts

Assuming a linear fall of J_c with T, we have:

$$T_{cs} = T_c - (T_c - T_0)\, J_m / J_{c0}. \tag{1.1}$$

If we suppose that the magnet is subject to a uniformly distributed disturbances, with a sudden release of energy which is uniform all along the winding, the temperature will rise adiabatically according to its the heat capacity.

It is possible to evaluate the amount of energy necessary for varying from T_0 to a critical value T_g, at which the magnet begins generating heat, by calculating the volumetric specific enthalpy between the two temperatures:

$$\frac{E}{V} = \gamma \mathrm{H}(T_{cs})\text{-}\gamma \mathrm{H}(T_0) \tag{1.2}$$

where V is the volume, gamma the density, enthalpy $H(T) = \int C_p(T)\,dT$, and $C_p(T)$ the specific heat at constant pressure.

Thus, material thermal properties of the winding contribute to the stability of a magnet.

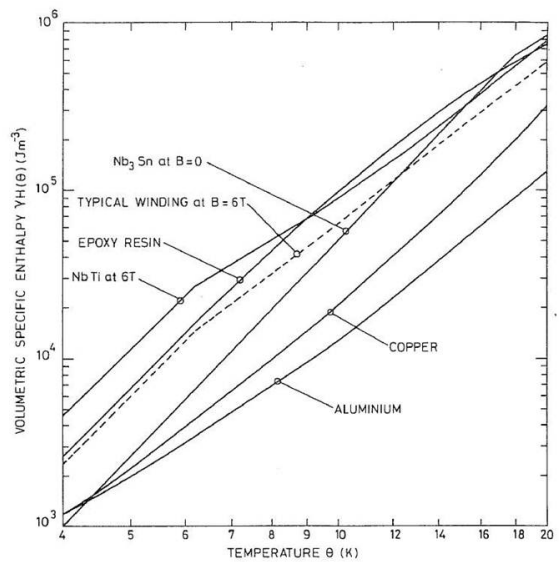

Figure 1.7: Volumetric specific enthalpy materials commonly used in magnets

1.2.4 Point disturbances

1.2.4.1 A wire purely of superconductor

We begin by considering a wire made purely of superconductor and a local "hot spot" which has been produced by a point disturbance in a wire carrying its critical current density J_c. Assuming that a certain amount of energy E increases the temperature of the superconductor above T_c over a length l, segment l of superconductor is dissipating power given by $J_c^2 \rho A l$ in [W], where ρ is the normal state resistivity, A the cross sectional area of the wire, and l the length of the normal zone. A portion (or all) of the heat is conducted out of the segment because of the thermal gradient, which can be approximated as $\frac{T_c - T_0}{l}$. Therefore, where k is conductivity $\left[W \cdot m^{-1} K^{-1}\right]$, when the power dissipated equals the power conducted away, we obtain:

$$\frac{2kA\,(T_c - T_0)}{l} = J_c^2 \rho A l \tag{1.3}$$

which results in

$$l = \sqrt{\frac{2k(T_c - T_0)}{J_c^2 \rho}} \tag{1.4}$$

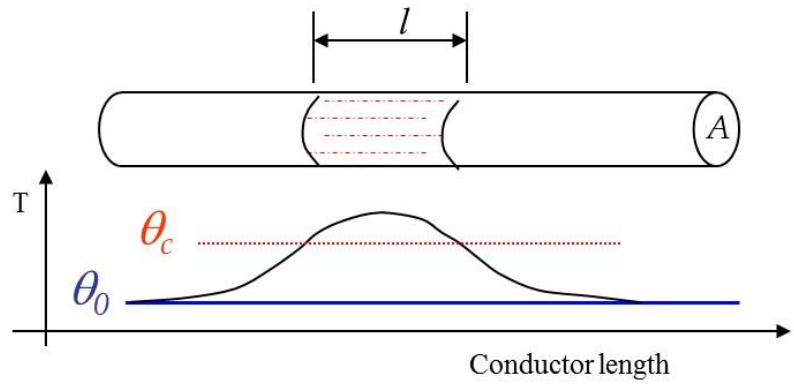

Figure 1.8: A small normal zone created by a point disturbance in a current-carrying wire [2]

The length l defines the MPZ, known as the minimum propagating zone. The length l is a property of the conductor in question, and may be used to characterize the type of disturbance. A normal zone longer than l will continue to grow (quench), whereas a normal zone shorter than l will collapse.

A wire made purely of superconductor, without any stabilizer (such as copper) quenches with nJ of energy. In order to increase l, since we do not want to reduce J_c, we have to increase $\frac{k}{\rho}$, meaning that we need a composite conductor.

1.2.4.2 Stabilization: superconductor surrounded by a metal

We now consider the situation where the superconductor is surrounded by material with low resistivity and high conductivity. Practical superconducting wires are made in composite form, containing both superconductor and normal conductor which is usually copper and sometimes aluminum. The simplest conductors were a single NbTi core surrounded by a copper jacket; at present composite wires containing many filaments of superconductor in a matrix of copper are manufactured because they improve stability and do not suffer from flux jumping (we will see after what kind on phenomenon is).

When the current density in a superconductor is raised above its critical value, the superconductor develops a resistance and the electric field rises steeply. The slope of the E-J line is known as the flux-flow resistivity because it is associated with the motion of flux vortices through the superconductor. Flux-flow resistivity is a function of temperature and magnetic field. In a composite conductor above its critical current, the current is shared between copper and superconductor, according to their resistivity. In practice the superconductor will continue to carry its critical current with almost all the excess transferring to copper. Heat is generated in both the copper and the superconductor. Usually, we are be concerned with the total power generation and it will be convenient to average this over the entire cross-section of the composite to obtain a generation G per unit volume, measured in W m^{-3}.

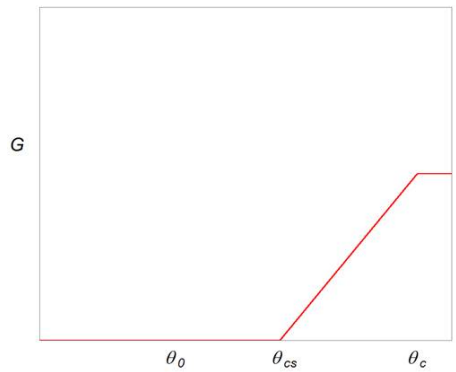

Figure 1.9: Temperature dependence of power generation in a composite conductor

So we have:

- $T < T_{cs} \longrightarrow G = 0$
- $T > T_c \longrightarrow G = G_c = \rho_{stab} \frac{\lambda^2 J_m^2}{1-\lambda}$
- $T_{cs} < T < T_c \longrightarrow G = G_c \frac{(T-T_{cs})}{T_c - Tcs} = \rho_{stab} \frac{\lambda^2 J_m^2 (T-T_{cs})}{1-\lambda(T_c-T_{cs})}$

where $\lambda = \frac{A_{sc}}{A_{tot}}$ and $J_m = \frac{I_m}{A_{sc}}$.

1.2.5 Minimum propagating zone

We now calculate the size of a minimum propagation zone (MPZ) within the winding of a magnet.

We modify the one-dimensional equation expressing $G(T)$ considered for the pure superconductor case, with a three-dimensional equation which includes the transverse conductivity.

Assuming the coil to be an isotropic continuum with two-direction conduction, i.e. cylindrical symmetry, the steady state equation of heat conduction becomes:

$$\frac{1}{r}\frac{\partial}{\partial r}(rk_r\frac{\partial T}{\partial r}) + \frac{\partial}{\partial z}(k_z\frac{\partial T}{\partial z}) + \lambda_w G(T) = 0 \tag{1.5}$$

where

- λ_w is the fraction in volume of the composite conductor (both superconductor and stabilizer) over the coil
- k_r is the conductivity along the wire
- k_z is the conductivity transverse to the wire.

The solution provides as MPZ an ellipsoid elongated in the z direction (along the cable), with a semi-axis R_g in z : $R_g = \pi\sqrt{\frac{k_z(T_c-T_{cs})}{\lambda_w G_c}}$ and a circular cross-section in the transverse plane with radius r_g : $r_g = R_g\sqrt{\frac{k_r}{k_z}}$.

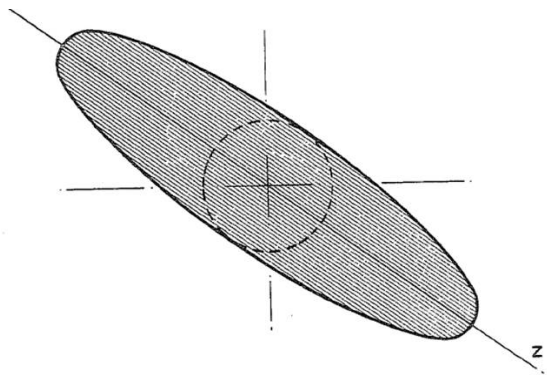

Figure 1.10: The ellipsoidal shape of a three-dimensional minimum propagating zone

1.3 Quenching and protection

1.3.1 Quench consequences

As we mentioned in the previous section the term "quench" is generally used to indicate the sudden transition from the superconducting to the normal, resistive state.

The basic process quench is the conversion of stored electromagnetic energy into heat. If this heat could be distributed uniformly throughout the magnet winding, the temperature growth is usually (but not always) be acceptable. Uniformity of heat distribution means little or no thermal stress. Unfortunately, the stored electromagnetic energy will never, in practice be spread uniformly around the magnetic winding. The quench always begins at a point and then spreads through the winding by a process of ohmic heating and thermal conduction. The resistance of this normal zone grows, as does its temperature. To limit this phenomenon, the power supply must be switched off and the energy must be dumped, with a rapid current decay. During this process the initiating point will always suffer the highest temperature rise because it is subjected to ohmic heating for the longest time. The local temperature rise may be sufficient to char the insulation or even melt the conductor, thus destroying the magnet. In less dramatic, still dangerous, cases it can causes thermal stress that weakens and degrades the coil.

In this section, we discuss current decay during a quench, the spreading of the normal zone, and the various techniques to protect the magnet from the dangerous consequences described above.

1.3.1.1 Temperature rise

We assume the quench initiates at a single point; in this part on the wind we will have a peak temperature. In the calculation, we shall assume local adiabaticity; we can hypothesize this because the quench time is fast: approximately less than a second and in certain cases les than 0.1 s, so the energy exchanged via conduction or by exchange to the helium bath is negligible.

We can consider the heat balance of unit volume of winding:

$$J^2(t)\,\rho(t)\,dt = \gamma C_p(T)\,dT \tag{1.6}$$

where all quantities are averages over the winding cross-section; γ is density and $C_p(T)$ is specific heat at constant pressure.

If we rearrange equation 1.6 and integrate we have

$$\int_0^\infty J^2(t)\,dt = J_0^2 T_d = \int_{T_0}^{T_m} \frac{\gamma C_p(T)}{\rho(T)} dT = U(T_m) \tag{1.7}$$

$U(T_m)$ containing only the properties of materials used in the winding, which may thus be used to calculate the maximum temperature T_m in terms of the initial current and T_d which is a characteristic time for the current decay following after the quench. T_d is the most important single parameter of a quench. If the current decays exponentially with a time constant τ we have: $T_d = \frac{\tau}{2} = \frac{1}{2}\frac{L}{R_{tot}}$.

We can also express the equation 1.6 as:

$$\frac{R(T)\,I(t)^2}{V}dt = \gamma C_p(T)\,dT \tag{1.8}$$

where R is the resistance, I is the current and V the volume. If we consider $R = \rho\frac{l}{A}$ where l is the length of the cable that has acquired a resistivity and $\rho = \left[\sum_{i=1}^{n_c}\frac{f_i}{\rho_i}\right]^{-1}$ where ρ_i and $f_i = \frac{A_i}{A_{tot}}$ are respectively the resistivity and the fraction of the i-th component and n_c is the number of components), $A = A_{tot}$ is the cross section of the conductor, we can rewrite 1.8 as

$$\rho(T)\left(\frac{I(t)}{A}\right)^2 dt = \gamma C_p(T)\,dT \tag{1.9}$$

mesured in [J/m^3].

By dividing 1.9 by the resistivity, and multiplying by A^2, we obtain:

$$I(t)^2\,dt = A^2\frac{\gamma C_p(T)}{\rho(T)}dT \tag{1.10}$$

mesured in [A^{2}s].

By integration over of 1.10 we obtain the so-called Quench Integral (QI):

$$QI(T_{peak}) = \int_0^\infty I^2(t)\,dt = A^2\int_{T_0}^{T_{peak}}\frac{\gamma C_p(T)}{\rho(T)}dT \tag{1.11}$$

mesured in [A^{2}s].

The Quench Integral is commonly measured in MA^{2}s, also known as MIITs ("mites"), which means 10^6(M), squared I $(I \cdot I)$, integrated in time (t).

Finally we can write the QI as a sum of two parts, by dividing the integral before and after the heaters (and the switch taking off the power supply) become effective (τ_d):

$$QI(T_{peak}) = \int_0^\infty I^2(t)\,dt = I_0^2\tau_d + \int_{\tau_d}^\infty I^2(t)\,dt \tag{1.12}$$

where τ_d is the total heater delay time, given by the quench detection time plus the quench heaters activation time (i.e. the time it takes for the heat transfer from the strip to the conductor, through the layers of insulation). The first term of 1.12 is trivial, since the current is kept constant by the power supply. The second term, in the case of a magnet protected by a dump resistance R_{Dump}, is given by the approximated exponential decay $I = I_0 \cdot \exp^{-t/\tau}$where $\tau = \frac{L}{R_{Dump}+R_{Quench}}$ mesured in [A].

1.3.1.2 Voltage distribution

When there is a quench the normal zone growth results in a rising resistance.

Before it is switched off, the power supply will attempt to maintain current until the coil voltage given by $R_{quench}(t) \cdot I$ is equal to the power supply voltage limit a voltage threshold on the power supply is used to diagnose a quench, and the power supply shut off. Once the power source is switched off, current begins to decay, and the inductive voltage balance $V_q = IR_q$ the resistive voltage: $L\frac{dI(t)}{dt} = I(t)\,R_q(t)$ where L is the self-inductance of the entire magnet.

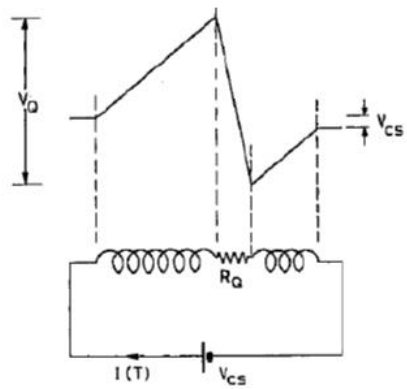

Figure 1.11: Voltage distribution in the circuit of a quenching superconducting magnet, before current source is switched off

1.3.2 Quench propagation velocity

We have seen previously that a thermal instability may lead to development of a quench.

A quench is characterized in its early state by:

- a normal zone propagating away from the initiation point
- a fast temperature rise in the normal region as Joule heat is deposited.

Quench propagates in a longitudinal direction, along the cable length, and in a transverse direction on the cable.

1.3.2.1 Longitudinal propagation velocity

We first consider a single wire: as regards the velocity in a longitudinal direction (i.e. parallel to the cable) the normal-superconducting boundaries are usually described by a plane thermal wave travelling at velocity v_l. This expression is obtained by solving the heat balance equation in the one-dimensional case and neglecting the thermal exchange in transversal direction:

$$v_l = \frac{J}{\gamma C_{av.met}} \sqrt{\frac{\rho_{av} \cdot k_l}{\triangle T}} \tag{1.13}$$

where

ρ_{av} and k_l represent respectively the electrical resistivity and the longitudinal thermal conductivity averaged over the unit cell.

We can also write 1.13 in an other way, using the Wiedmann-Franz law:

$$v_l = \frac{J}{\gamma C_{av.met}} \sqrt{\frac{L \cdot T_m}{\triangle T}} \tag{1.14}$$

in this case

- $\triangle T = T_m - T_0$ where $T_m = \frac{T_g + T_c}{2}$, T_0 is the operation temperature of the magnet, T_g is the temperature at which ohmic heat generation begin (critical generation tempereture) and T_c is the critical temperature at J=0.

- J is the current density.
- $\gamma \cdot C_{av.met.}$ the volumetric specific heat averages over the metallic part of the unit cell
- L the Lorentz number.

Note that the quench propagation velocity is a function of the temperature margin.

1.3.2.2 Transverse propagation velocity

For the transverse propagation velocity, we consider a solenoidal winding: the heat produced by ohmic dissipation diffuses through the insulation in transverse direction, i.e. perpendicularly to the cable itself. For each quench propagation velocity in the transverse direction:

$$v_t = v_l \cdot \frac{(\gamma \cdot C)_{av.met.}}{(\gamma C)_{av.}} \cdot \sqrt{\frac{k_t}{k_l}} \tag{1.15}$$

where$(\gamma C)_{av.}$ is the specific volumetric heat averaged over the total cross section, while $(\gamma \cdot C)_{av.met,}$ is averaged over the metallic part only. Tipicaly $\frac{k_t}{k_l} = 10 - 4$, so v_t is about 1% of v_l.

1.3.3 Protection methods

The steps descibed thus far are:

1. The magnet is superconducting and at some state $I = I_{0.}$
2. Quench initiation: a quench occurs at some location in the magnet and as the normal zone propagates, a resistive voltage is generated
3. Quench detection: the detection system determines the existence of a quench once voltage has developed; a time $\triangle t_{det}$ has elapsed.
4. Switch off the power supply: as soon as the quench is detected, the first action to be taken is to disconnect the current supply, by opening a switch and deriving the magnet current into an exteral dump resistor. The current in the magnet begins to decay with a time constant $\tau = \frac{L}{R_{tot}}$ (where remember we have seen in 1.3.1.1 the resistence R_{tot} is the sum of internal normal zone resistance and any external dump resistor connected to the system, and L is the total system inductance $E = \frac{1}{2}LI^2$).
5. Trigger heaters (usually at the same time of point 4): is an active method to spread the quench quickly over the whole (or a large fraction of) coil.
6. Quenchback: another heat dissipation mechanism, in addition to the active quench heaters, may be triggered by the quench itself. They are called quench back because in return they speed up the quench propagation, usually favouring a more homogenous distribution of the energy.
7. Magnetic energy is converted into heat: partly goes into the coils, increasing the temperature, and partly is dumped on the external resistor.

For most accelerator magnets the natural normal zone growth is not sufficient to provide a fast resistance growth: in such a case the decay time is too long and the MIITs may become dangerously high. The methods for enhancing the resistance are:

1. Add an external dump resistor
2. Induction of coupled secondary circuit (s)

(a) May take the form of a shorted secondary or coil subdivision

(b) Mutual inductance between coil and secondary circuits results in voltage and hence dissipation of energy in secondary circuits

(c) Provide quenchback mechanism.

3. Force most of the magnet to quench by applying heat by means of:

(a) Heaters (therefore called quench protection heaters), that can be tailored to the magnet

(b) Heater circuity designed to provide fast thermal rise with reasonable voltages

(c) Thermal diffusion time for heat to pass quickly from heater to coil is critical.

1.3.3.1 External dump resistor

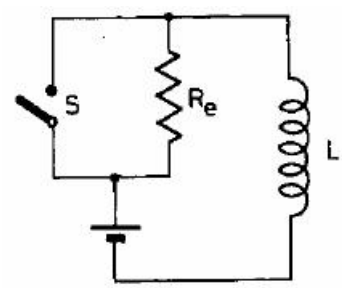

Figure 1.12: Protection by means of switched external dump resistor

The simplest enhancement of the quench protection is the addition of an external (dump) resistor R_e. When the start of a quench is detected, S (the switch) opens and the current decay through R_e.

The law of current decay is (neglecting the internal R_{quench}):

$$I = I_0 \exp\left(-R_e t/L\right) = I_0 \exp\left(-t/T_e\right) \tag{1.16}$$

so that

$$\int J^2 dt = \frac{L I_0^2}{2A^2 R_e} = \frac{I_0^2 T_e}{2A^2} = U\left(T_m\right). \tag{1.17}$$

where A is the total cross section of the cable.

The maximum external voltage is given by $V_e \leq I_0 R_e$. This poses a limit to the protection by an external resistor the voltage must not be too large or there will be problems of insulation breakdown in the magnet or at other places around the circuit at the time of the switching. A breakdown in that moment, when all the energy is still stored in the magnet is catastrophic for the magnet itself.

1.3.3.2 Induction of coupled secondary circuit (s)

In accelerator magnets this technique is not used. However we can consider as couped secondary circuit the metallic pieces coupled with the coils, i.e., submitted to varying magnetic field. The dissipation in these pieces subtract energy from the magnets, contributing to current decay.

1.3.3.3 Active protection using heaters

For the protection of a magnet with very high current density such as an accelerator magnet, a common method is application of active heaters, called quench heaters, directly on the coil in order to quickly spread the quench in the coil. Heaters are typically thin strips of stainless steel sandwiched between two thin insulating foils and covers the external surface of the coils. A detailed description of the heaters used in our experiment is described in the subsection 3.2.3.

Chapter 2

LARP Long Nb_3Sn Quadrupole Design

2.1 Introduction

What is a Quadrupole? We begin with a brief description of the main characteristic of a quadrupole. Because of the high velocity of charged particles in medium and high energy accelerators, magnetic deflection is much more powerful than electrostatic, and use the Lorentz force:

$$\mathbf{F} = q\,(\mathbf{v} \times \mathbf{B}) \tag{2.1}$$

This force is enabled by various magnets that make up "the lattice" required to bend, steer and focus a charged particle beam. The quadrupoles in the lattice are of two types: "F quadrupoles" (which are horizontally focusing but vertically defocusing) and "D quadrupoles" (which are vertically focusing but horizontally defocusing).The overall effect on the beam is focusing in both the horizontal and vertical planes. We can obtain a focusing function using a structured known as a "FODO lattice" consisting of a basis of a focusing quadrupole F, "nothing" (i.e. drift space with respect to focusing effect, often a bending magnet), a defocusing quadrupole D and another length of "nothing".

In the middle axis of a quadrupole the magnetic field is zero, which then increases linearly with the radius. The central trajectory of the particles is ideally along the axis of the quadrupole. A particle with an offset trajectory , i.e. that it doesn't cross the quadrupole in the center, is subject to a force bending the particle toward the centerline, in the focusing plane. The field grows proportionally with the length of the radius and the strength of the force. A quadrupole is characterized by its gradient $G = \frac{dB}{dx}$ (where x is the transversal direction respect to the particle direction), since it is the gradient that determines the focusing strength.

Fermilab's [3] quadrupoles do not have exactly the functions of the normal FODO lattice - they are placed next to the detectors for - focusing the particle beam inside the experimental detectors. To increase the collision rate, (one of the most important goals of a particle collider, also called "luminosity"), the beam must be squeezed as much as possible at the interaction point. LHC [4] already has very powerful quadrupoles to achieve this squeezing which are referred to as low-beta quadrupoles. Fermilab's quadrupoles are designed to maximize this squeezing, allowing an increase in the number of collisions, i.e., the luminosity of the LHC. These quadrupoles are the heart of the project "High Luminosity LHC" (HL-LHC), which will represent a major upgrade to take place around.

The development of Nb_3Sn magnets for particle accelerators goes back to the 1960's: however a practical use was never attempted, because of the difficulty of the technology. A larger effort on

Nb_3Sn was carried out at the end of the 1990's, but it is only with LARP (the USA LHC Accelerator Research Program) that a systematic and continuous R&D has been initiated. LARP is leading this effort, which aim at developing a full size model of the Interaction Region, i.e. low-beta quadrupole for achieving the luminosity upgrade of the Large Hadron Collider at CERN. The model must have a combination of gradient and aperture such as that the peak field is at least 40-50% higher than the present quadrupoles which have been constructed in Nb-Ti. Fermilab's LARP magnet is the first 4m long Nb_3Sn quadrupole magnet ever built and features an aperture of 90 mm (LHC low-beta has a 70mm aperture). The design of Fermilab's magnet, called LQ (Long Quadrupole, see Figure 2.1), is based on the LARP Technological Quadrupoles (TQ, in two variants: TQC and TQS) whose development was carried out in the first years of LARP, 2005-2008.

Before providing a description of the Long Quadrupole project, we will describe superconducting magnets for particle accelerators in general and the basic properties of Nb_3Sn, with a sub-sections dedicated to multifilament wires and superconducting cables.

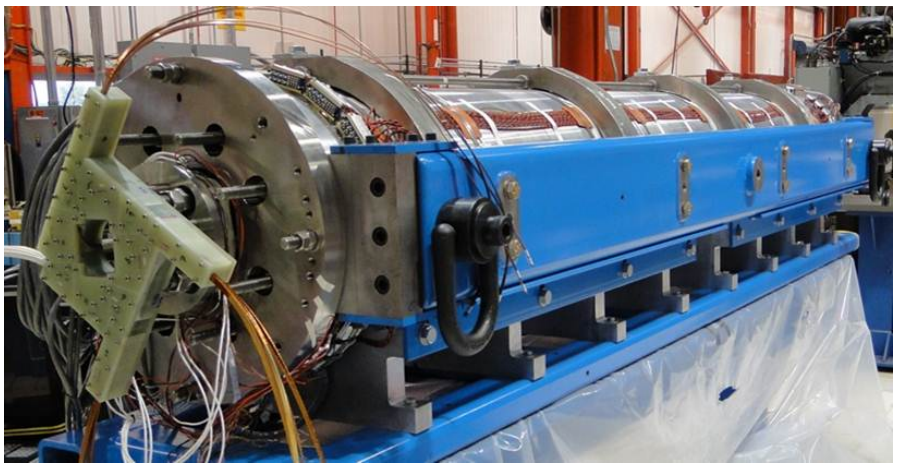

Figure 2.1: LQS01b

2.2 Nb_3Sn Superconducting Magnets for Particle Accelerators

2.2.1 Superconducting magnets for particle accelerators

Particles can be accelerated to high energy by means of linear or circular accelerators.

In a linear accelerator (linacs) particles are accelerated in a straight line against a target at one end or by shooting at beam against a similar beam accelerated by a second linac, such as the International Linear Collier [5]. Linacs are often used to provide the low-energy first acceleration stage to a particle beam-before the particles are injected into a circular accelerator. In a circular accelerator particles move in a circle, maintained in orbit by the centripetal force provided by a magnetic field, until they reach maximum energy. We know by the laws of the classic mechanics that $\frac{mv^2}{R} = q \cdot v \cdot B$ so $p = q \cdot R \cdot B$. In relativity, the momentum p is $p_{rel} \approx \frac{E_k}{c}$ where E_k is the kinetic energy and c the celerity. By combining the two equations, we obtain $\frac{E_k}{q} = c \cdot R \cdot B$ mesured in [eV] so, the energy or momentum magnetic field is governed by the following law:

$$E = 0.3 \cdot B \cdot R \tag{2.2}$$

where E is the energy of the particle in GeV, B is the magnetic field in Tesla and R is the radius in meters.

The first large particle accelerator based on superconducting magnets of about 4T was the Tevatron at Fermilab, which began operation in 1983. After the LHC reached energy greater than Tevatron in December 2009, Tevatron was turned off in 2011. LHC superconducting magnets are wound with Nb-Ti and operate at 1.9 K providing a field of 5 Tesla (delivering proton collision at 4-4 TeV) and eventually its magnets will reach 8.3 T, allowing collisions at 7-7 TeV.

2.2.2 Basic properties of Nb_3Sn

2.2.2.1 Multifilament wires: Motivations and Fabrication

The superconducting materials used in accelerator magnets are:

- subdivided into small-diameter filaments($5 - 20\,\mu m$).
  - to reduce flux jump effects
  - to minimize field distortions caused by superconductor magnetization
- twisted together
  - to reduce inter-filament coupling and AC losses

and

- embedded in a copper matrix
  - to provide basic adiabatic stability
  - to protect the superconductor after a quench
  - to reduce magnetic instabilities called flux jumps.

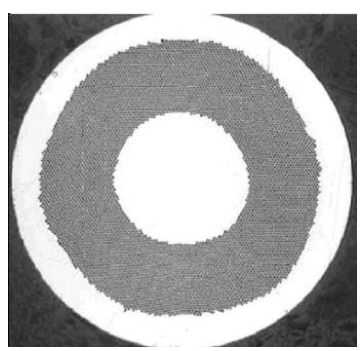

Figure 2.2: NbTi LHC wire section [6]

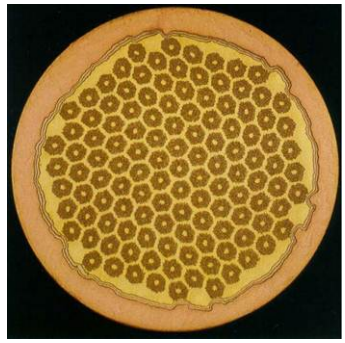

Figure 2.3: Nb_3Sn bronze-process wire [6]

Before describing the multifilament wires in more details, it is important to better understand the varied motivations for constructing them. For this, we first provide a short summary of the physics phenomena set forth above.

Flux jumps are sudden redistributions of the magnetic flux, which happening when an external magnetic field penetrates a type-II superconductor in the mixed state. In this state the flux in the superconductors is quantized and a single quantum flux (a bundle of magnetic lines surrounded by a vortex of superconducting current) is called fluxoid. The fluxoid distribution depends on the applied magnetic field and on the current J_c. If the superconductor is subjected to a thermal disturbance, the local change in J_c produces a redistribution of the flux; indeed, a well verified model (a critical state model) predicts states that J is either zero or J_c. If J_c changes, B distribution also changes, since $J = \frac{dB}{dx}$ according to Ampère's law. But a change in flux distribution in a superconductor means a rearrangement of the fluxoids, i.e., a motion or "jump" of fluxoids, which is accompanied by power dissipation. High conductivity copper greatly reduces this instability.

We also mentioned the phenomenon of superconductor magnetization. When a filament is in varying external fields, its inner parts are is shielded by a current distribution in the filament periphery. These shielding currents are proportional to the amplitude of the applied field and, since we are in superconductor, they do not decay when the external field is held constant.

Major is the diameter of the filament is large and major is the magnetic dipole due to this shielding current is lager and so magnetic disturbance for the particle trajectory.

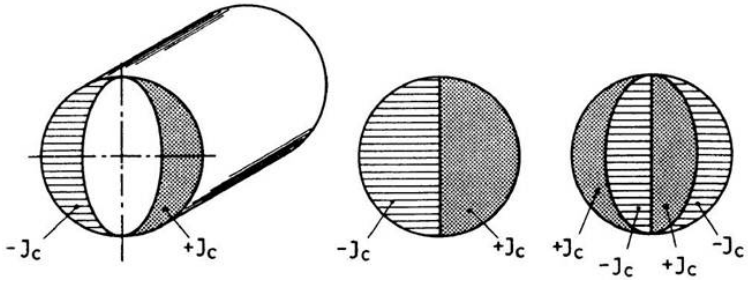

Figure 2.4: Superconductor magnetization [7]

Of a different origin is the phenomenon of inter-filament coupling. This happens when a multifilamentary wire is subjected to a time varying magnetic field and current loops are generated between filaments.

It can be demonstrated that the coupling of even narrow filaments can produce larger magnetic dipole. To avoid this problem, the conductor has to be twisted, in order to drastically reduce the coupling effect.

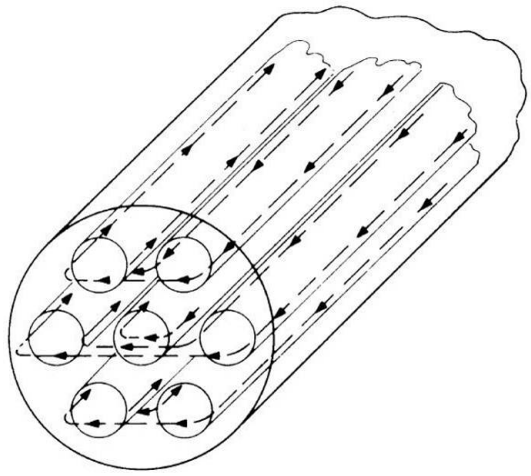

Figure 2.5: Composite conductor with filaments completely coupled [1]

We also provide a brief discussion about quench protection (this is describe in more details in 1.3.3). Superconductors have a very high normal state resistivity. It can be shown that a filament of NbTi, if quenched, could reach very high temperatures, and even melt out, in few milliseconds. If the filament is embedded in a copper matrix, when a quench occurs, the current redistributes in the low-resistivity matrix and the peak temperature can typically be maintained below 300 K. The copper matrix facilitates quench protection because it allows the quench to propagate and it provides time to act through a protection circuit. The copper needs to be of very low resistivity, i.e., pure and annealed-this mean in practice an $RRR = \frac{\rho_{300K}}{\rho_{4K}}$ of 100 (typical values range between 60 and 200). In the case of a small volume of superconductor heated beyond the critical temperature (for instance because of a flux jump), the current can flow in the copper for a short moment, allowing the filament to cool (via thermal conduction along the wire and/or via heat exchange with the cryogenic fluid) and eventually allowing the recovery of superconductivity. Note that a conductivity matrix also helps stabilize the conductor against flux jumps.

Fabrications of Ni-Ti alloy multifilament wires and Nb_3Sn inter-metallic compound multifilament wires are different, because the two materials have different properties. I will describe just the fabrication of Nb_3Sn because the LQ magnet is wound with wires made out of this material.

Nb_3Sn is a brittle material. The precursor wire is not brittle, but the wire needs to be treated (or reacted) at high temperature (650-700 °C) in order to form the inter-metallic compound. Unlike NiTi that can be extruded, drawn, and then wound easily, Nb_3Sn must be formed during the last step of the fabrication of the cable or the coil. If it is formed at the end of cable fabrication and then is wound, the process is referred to as React & Wound (R&W). If it is first wound and then the entire coil is reacted, the process is called Wind & React (W&R). Fermilab's coils are such that only W&R is possible, which puts severe stress on the electrical insulation that must withstand a 700 °C treatment without degrading.

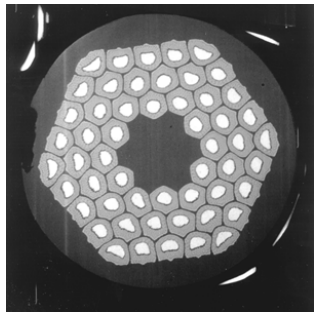

Figure 2.6: Nb_3Sn wires

The process requires several steps:

- Assembly of multifilament billets from Nb_3Sn precursors (CuSn and Nb).
- Fabrication of the wire through extrusion-drawing technique.
- Fabrication of the cable.
- Fabrication of the coil:
  - "Wind & React" : first coil winding and then formation of Nb_3Sn.

During the "reaction", the CuSn and Nb are heated to about 600-700 C in a vacuum or inert gas (Argon) atmosphere. The Sn diffuses in the copper first (forming bronze) and then into the Nb filaments where it reacts to form Nb_3Sn compound.

There are two main processes for forming Nb_3Sn wires - the bronze process and - the internal tin process (ITD). This last has three variants, the most well known begin classical ITD: the powder in tube (PIT) process and the Rod Restacking Process (RRP). Other types of ITD technology, such as the modified Jelly Roll, have now been abandoned.

For the bronze process, Nb rods are inserted in a bronze (CuSn) matrix. The pure copper is placed in the periphery and protected with a diffusion barrier (Ta) to avoid contamination by tin atoms which then maintains high RRR at cold.

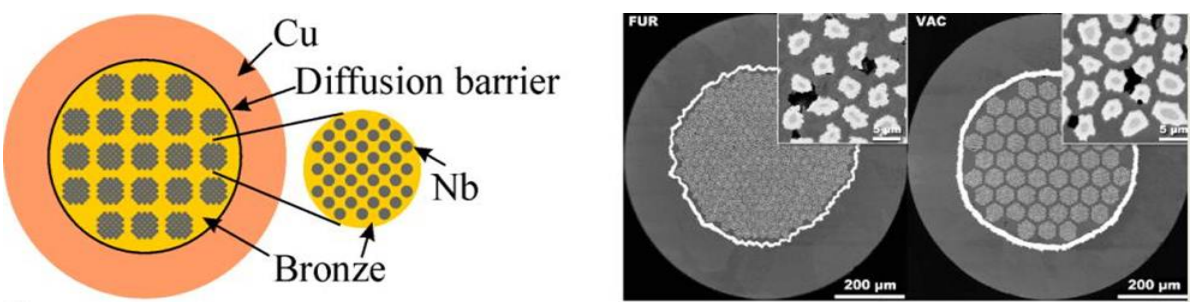

Figure 2.7: Bronze process [8]

The advantage is a small filament size, but the disadvantage is the limited amount of Sn in bronze and the necessity of annealing steps during wire fabrication to recover the bronze's ductility.

In the internal tin process: a tin core is surrounded by Nb rods embedded in Cu (Rod Restack Process, RRP) or by layers of Nb and Cu (modified Jelly roll), forming an element or island. During reaction the tin diffuses at low-intermediate temperature into the copper, forming a very

tin-rich bronze. Then, at the temperature plateau (650-700 °C) the tin diffuses into the Nb. Many subelements are included in a single wire and each sub-element has a diffusion barrier, Nb or Ta, to preserve the purity of the stabilizing copper. The advantages are that there is no need for annealing steps and the large amount of Sn yields potentially more J_c, but the disadvantage is that the small filament spacing results in a large effective filament size (100 μm) with consequent large magnetization effect and instability.

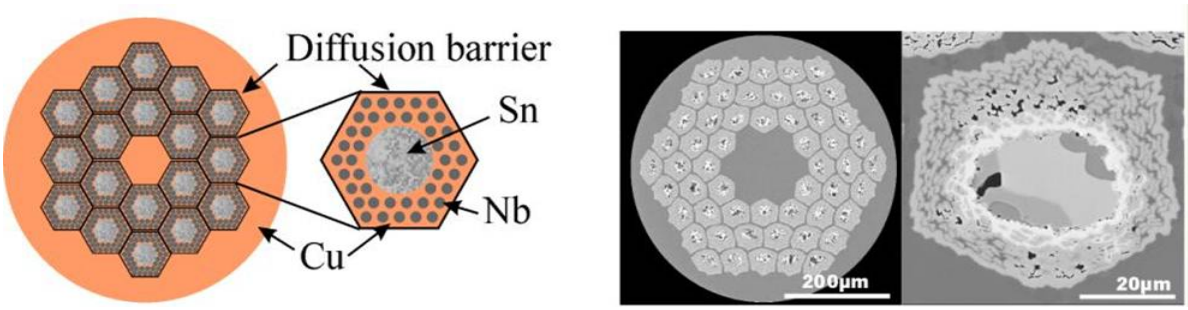

Figure 2.8: Internal tin process [8]

A variant of the ITD is the powder in tube (PIT) process. An Nb tube is filled with $NbSn_2$ powder and then fitted into a copper tube. Here bronze is not formed because during the thermal treatment the tin atoms diffuse directly into the Nb tube. The reaction time is calculated so that not all of the tin diffuses into the all Nb tube, leaving an unreacted ring at the outer part of the Nb tube. This unreacted acts as a barrier preserving the purity of the external copper. By assembling many of these tubes one can create a wire with a relatively small filament size (30-50 μm). Another advantage of PIT over the classical ITD is the short heat treatment (resulting from the proximity of tin to Nb and omission of the bronze phase), but on the other hand PIT involves a higher fabrication cost and somewhat smaller J_c.

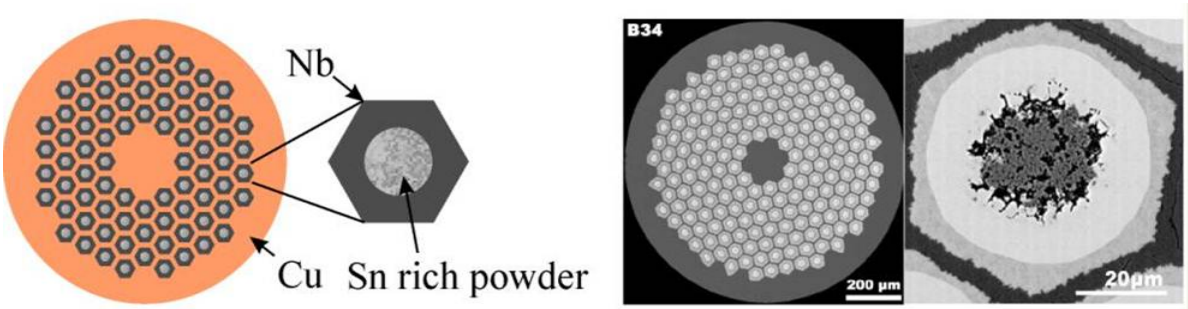

Figure 2.9: Power in tube (PIT) process [8]

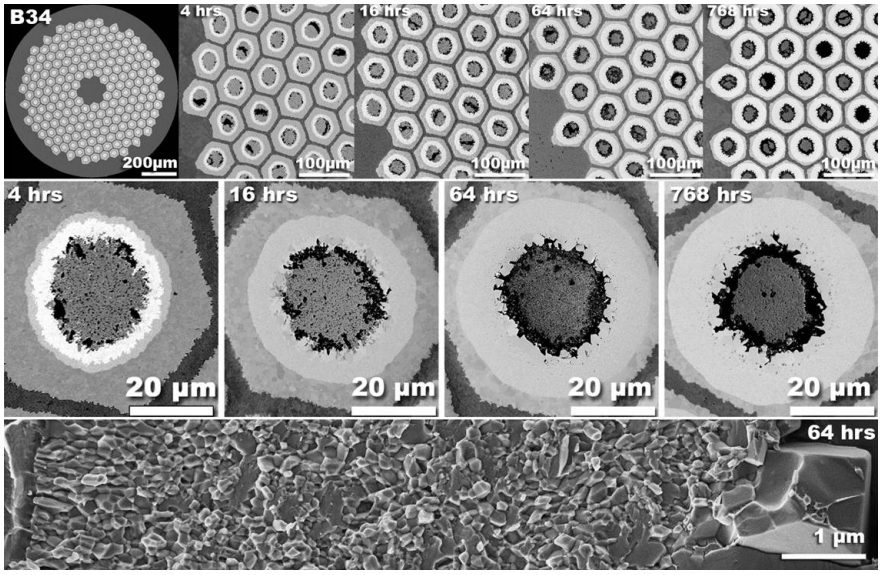

Figure 2.10: Reaction of a PIT wire [8]

2.2.2.2 Superconducting cables

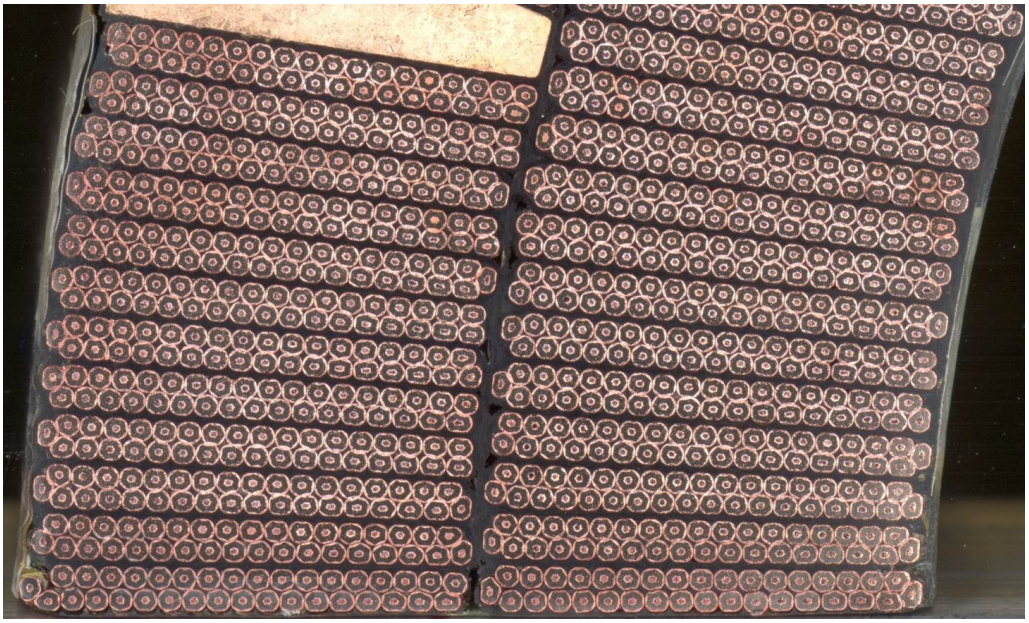

Figure 2.11: Superconducting cables

Most of superconducting accelerator magnets are made from a multi-strand cable of the so-called Rutherford type, sketched in the picture below:

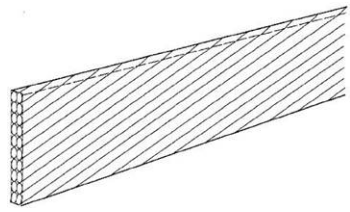

Figure 2.12: Rutherford cable [6]

The wires are twisted and compressed into a flat two-layer cable. The cable is usually permeable to liquid helium so the surface of all strands is wetted with the coolant. The advantages of a multi-strand cable are the possibility of achieving a large current, easily modulable according to the design and a reduction of the number of turns which facilitates coil winding and reduces coil inductance. Small inductance is very important for quench protection because enable a fast current discharge and requires less voltage at the power supply during current ramp-up. The cable is twisted, i.e. each strand is transposed to reduce interstrand coupling currents and provide more mechanical stability.

How is a Rutherford cable fabricated?

Rutherford cables are fabricated by means of a cabling machine: strands are wound on spools mounted on a rotating drum and they are twisted around a conical mandrel into an assembly of rolls (Turk's head). The rolls compact the cable and provide the final shape.

The final shape of a Rutherford cable cross section can be rectangular or trapezoidal. The cable design parameters are:

- Number of wires (strands)
- Strand diameter
- Cable mid-thickness
- Cable width
- Pitch length
- Pitch angle (when the cable has a trapezoidal shape)
- Cable compaction (or packing factor).

The cable compaction is chosen to provide good mechanical stability and high current capability, while at the same time leaving enough space for helium cooling or epoxy impregnation. However cable compaction, if too high, is one of the primary factors causing strain induced critical current degradation.

In a degradation scenario, the strands are deformed on the cable slides. This deformation may induce a breakage of the reaction barrier and a tin leak which can cause a poisoning of the copper purity and an incomplete Nb reaction. Qualitative assessment of the degradation may be efficiently conducted by measuring after cabling the edge facets.

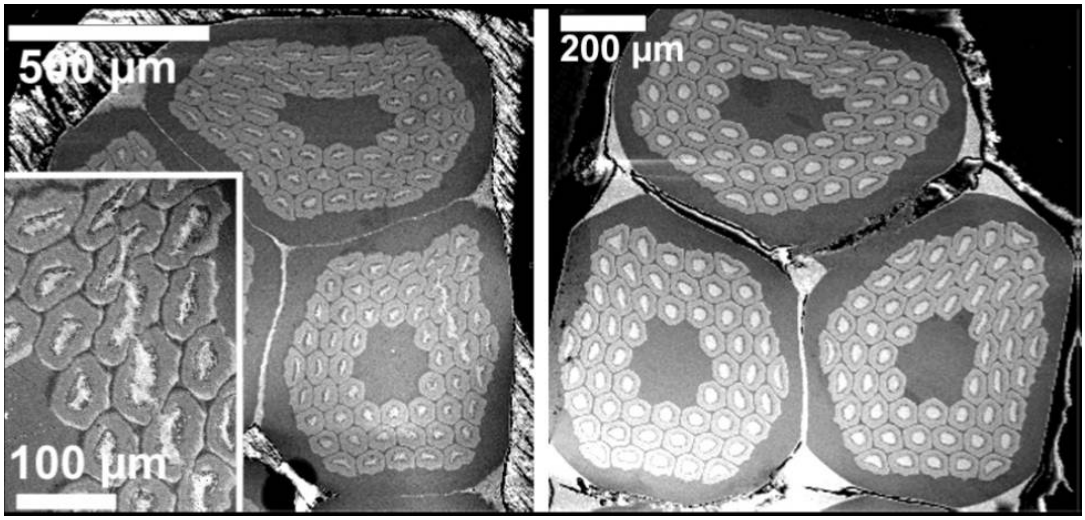

Figure 2.13: Deformation Rutherford cable [9]

In the Figure 2.13 on the left shows a serious edge deformation and on the right shows a harmless edge deformation.

Finally there is the insulation step - in Nb_3Sn magnets, where cable is reacted at 650-700°C, the most common insulation is a tape or sleeve of special fiber-glass. Typically the insulation thickness varies between 100 and 200 μm.

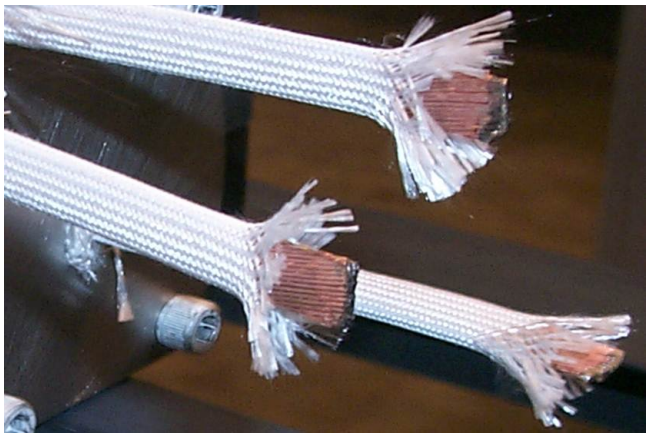

Figure 2.14: Insulation cable with a fiber-glass

2.3 The Long Quadrupole

2.3.1 Magnet Design

[1]The design of the Long Quadrupole (LQ) is based on the design of the Technological Quadrupoles. In the TQS (Technological Quadrupoles with Al shell) the iron is closer to the coil than in the TQC (Technological Quadrupoles with Collars), resulting in a slightly better load line and more sensible saturation effects.

[1]This Section refers to [10]

The main parameters of both designs are summarized in Table 2.1 (assuming a critical current of $2,400\ A/mm^2$ at 4.2 K, 12 T).

Table 2.1: Long Quadrupole magnet parameters based on TQ designs

Parameter	Unit	TQC	TQS
N of layers	-	2	
N of turns	-	136	
Coil area (Cu + nonCu)	cm^2	29.33	
4.2 K temperature			
Quench gradient	T/m	221.4	234
Quench current	kA	13.34	13.2
Peak field in the body at quench	T	11.48	12.0
Peak field in the end at quench	T	11.94	11.8
Inductance at quench	mH/m	4.56	5.03
Stored energy at quench	kJ/m	405.7	438
1.9 K temperature			
Quench gradient	T/m	238.43	252
Quench current	kA	14.44	14.4
Peak field in the body at quench	T	12.37	12.9
Peak field in the end at quench	T	12.87	12.7
Stored energy at quench	kJ/m	472.1	511

The cable for the LQ magnets is fabricated using the Rod-Restack Process (RRP) wire from Oxford-Instruments Superconducting Technology (OI-ST). Strand diameter is nominally 0.7 mm and is of the 54/61 design (54 subelements in a stack pattern of 61).

Table 2.2: TQ/LQ cable parameters

Parameters	Units	TQ Final	Tolerance
Strands in cable	No.	27	NA
Strand diameter	mm	0.7	+/- 0.002
Width	mm	10.077 max.	+0.000, -0.100
Thickness	mm	1.26	+/- 0.010
Keystone angle	deg.	1.0	+/- 0.10

To balance the needs of a J_C (12 T, 4.2 K) of about $2,800\ A/mm^2$ and a RRR greater than 100 (to assure stability at low field) the present TQ02 coil heat treatment schedule is 72 h at $210^{\circ}C$, 48 h at $400^{\circ}C$, and 48 h at $640^{\circ}C$. Strands with this heat treatment have a stability current greater than 1,000 A at 4.2 K. This current meets the LARP program target of having the stability current double the strand short sample current in a magnet. The cable parameters to be used in LQ are identical to those that have been developed for TQ magnet.

Table 2.3: LQS01 magnet parameters

Jc at 12 T, 4.2 K	Temperature	Current	Gradient	Layer 1 Peak field	Layer 2 Peak field	Stored Energy	Inductance
A/mm^2	K	kA	T/m	T	T	kJ/m	mH/m
2400	4.5	13.175	230.3	11.776	10.083	427.4	4.9
2400	4.2	13.369	233.4	11.936	10.217	439.3	4.9
2400	1.9	14.500	251.3	12.867	10.992	512.1	4.9
2800	4.5	13.785	240.0	12.279	10.502	465.4	4.9
2800	4.2	13.989	243.2	12.447	10.642	478.6	4.9
2800	1.9	15.180	262.1	13.425	11.458	558.5	4.8

2.3.2 Coil design and fabrication

The LQ coils are fabricated using the Wind-and-React method. The inner and outer layers of a coils are wound without a splice between the layers, using the same piece length of cable, and are cured together.

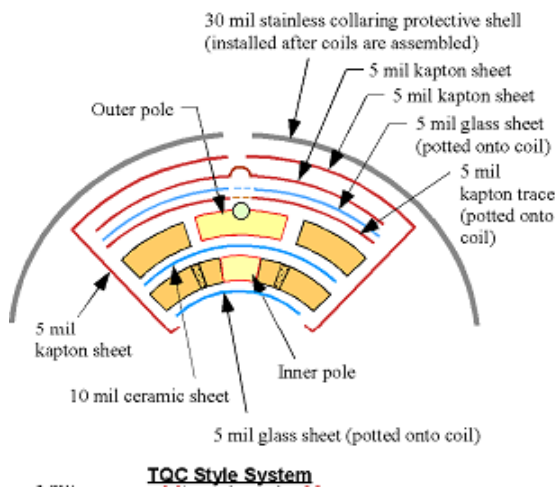

Figure 2.15: Cross section of LQ coil with TQC ground insulation system

The cables used for the first LQ model (LQ01) are insulated by ~0.1mm thick S-glass sleeve. The sleeve is reinforced by palmitic acid sizing applied after burning the original sizing. The use of S-glass insulation braided directly to the cable is under development for possible use in subsequent models.

A ceramic binder is applied after winding the inner coil layer. The layer is subsequently cured under pressure in a precise mold at 150°C in air for 30 minutes subjected to an azimuthal pressure of approximately 35 MPa. The outer layer is wound above the cured inner layer and the curing operation is repeated. The coils are heat treated in argon atmosphere, and then vacuum impregnated with CTD101k epoxy resin.

LQ coils are wound around a pole (sometimes referred to as an "island") made of Ti-Al-V. The use of this material, which has a very low thermal dilation coefficient, avoids the need of gaps in the pole during the heat treatment, and is more compatible with the longitudinal thermal dilation of a TQS-style structure. The ground insulation is made of overlapping layers of polyimide (Kapton®) sheets (127 μm thick) as in present TQC coils (see in Figure 2.15). The amount of ground insulation is equivalent to that used on the present LHC IR quadrupoles.

Protection heaters cover the entirety of the inner and outer coil surfaces. Together with the wiring for the voltage taps, the protection heaters are glued between two layers of Kapton (the resulting sandwich is called a "Trace"). After tests at 1.9 K the inner surface of TQ coils presented several "bubbles" (local detachment of the insulation from the conductor), possibly caused by vaporization of helium that, in its superfluid phase had penetrated through the epoxy impregnated insulation. These bubbles reduce the efficiency of protection heaters located on the coil inner surface. The placement of protection heaters (without Kapton) between the coil layers is a possible solution to this problem. Otherwise, the first LQ could be tested at 4.5 K and 2.3 K avoiding superfluid helium.

2.3.3 Mechanical design

The structure for the first LQ could be considered a simple extension of the 1 m long TQS magnet; like the TQS, the LQ is based on an aluminum shell pre-tensioned with pressurized bladders.

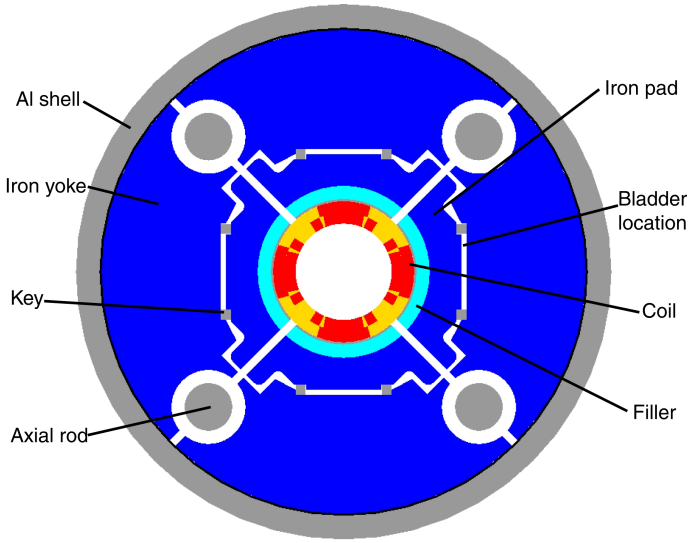

Figure 2.16: TQS02 cross-section

The design comprises an iron yoke surrounded by a 20 mm thick aluminum shell, and includes four pads and four coils wound around titanium poles. Between each pad and the yoke, two interference keys are used to balance the azimuthal tension in the outer shell with the azimuthal compression in the inner coils.

The 3D design (see Figure 2.17) is characterized by:

- Stainless steel or iron pad laminations (50 mm thick)
- Iron masters (1.6 m long)
- Iron yoke laminations (50 mm thick)
- Four aluminum shell segments (0.820 m long)
- Axial rods and tie rods 3.3 m long

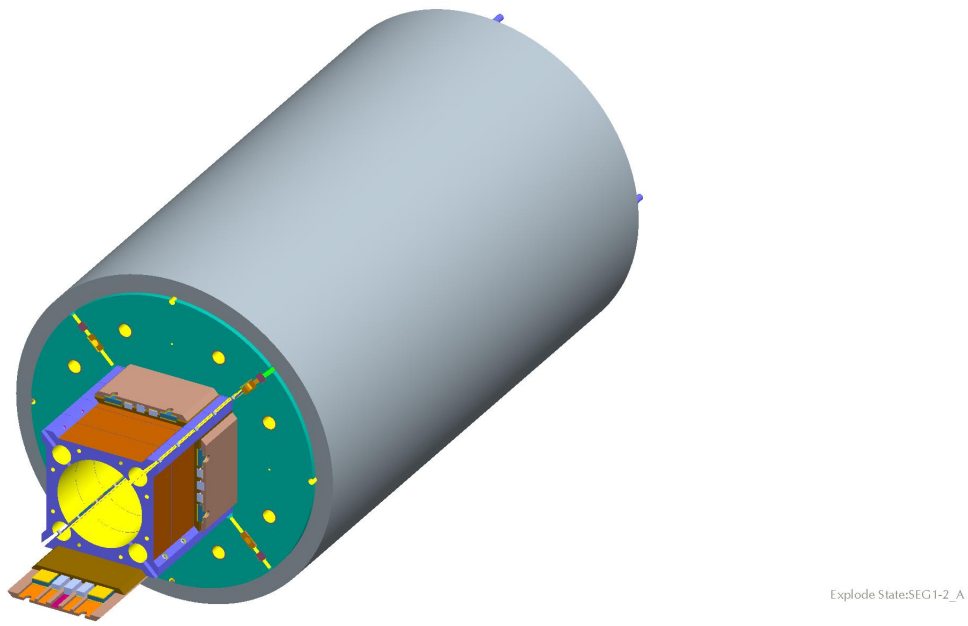

Figure 2.17: 3D view of pads, masters, yoke, and shell

Chapter 3

Quench Protection of the Long Quadrupole

3.1 Introduction

LQS01a, the first long Nb_3Sn quadrupole made by LARP, was cold tested in December 2009. The LQS01a training was stopped after reaching the target gradient of 200 T/m (short sample was evaluated to be about 240 T/m) , in order to avoid possible coil damages, because cool down and test data showed not adequate coil pre-stress.

The reassembled magnet LQS01b was delivered to the Fermilab's vertical magnet test facility (VMTF) on June 8th, 2010. After it was electrically checked, magnetic measurements at room temperature were carried out and then it was cool down at liquid helium. Once test finished test, LQS01b was removed from the VMTF cryostat on September 13th, 2010.

In this chapter we will make a briefly description of the instrumentation and the test results of this magnet, followed by a description of the protection design and, finally, a description of the codes used for quench simulations.

3.2 Quench Protection [1]

3.2.1 Protection design

The goal of quench protection is to convert safely magnetic energy into heat, while minimizing hot spot temperature and peak voltages. Protection strategies rely on various methods; the active protection uses an external resistance like we have seen in 1.3.3.1, and protection heaters, as shown in 1.3.3.3.

3.2.2 LQS01b Instrumentation

Voltage tap covered the inner and outer layers, pole turn, multiturn and splice sections. There were 13 voltage taps on the inner layer and 7 voltage taps on the outer layer, as it is shown in Figure 3.1.

[1] This Section refers to [11]

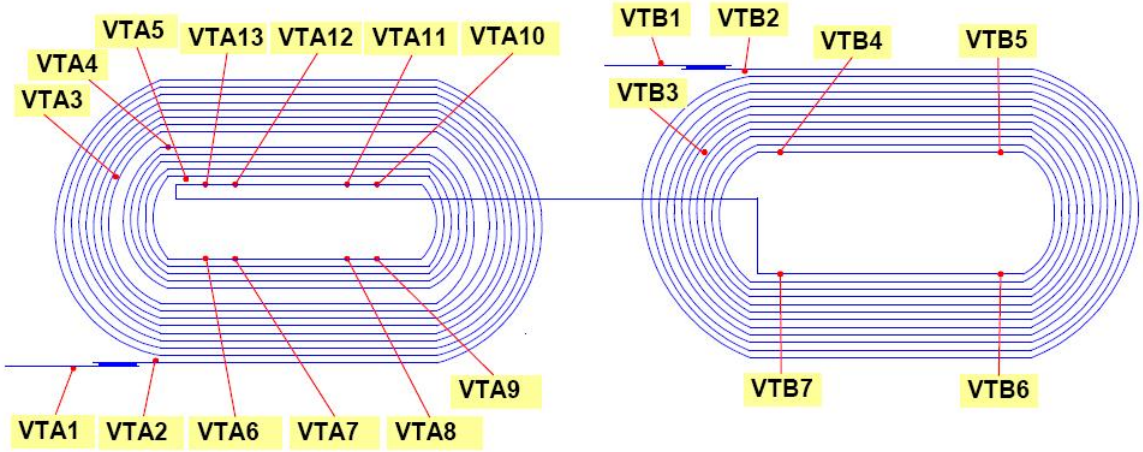

Figure 3.1: LQS01b voltage taps location for the inner (left) and outer (right) layers

Finally we have quench antenna for localization of quenches. Quench antenna consists of small coils mounted on the tube that contains the coil magnetic measurements system. The magnetic measurement system tube is inserted inside the magnet bore and is usually rotated to measure the magnetic field content of the magnet. During the training test this measurement system is kept still: in this way the small coils can detect the small current redistribution that happens at the beginning of the quench. The quench antenna is a particular arrangement of these small coils in a way that they are capable to trace the coils and the layer when the quench is started and the longitudinal position.

3.2.3 Protection heaters

Each coil is equipped with 4 protection heaters and 1 spot heater. Protection heaters are installed on both the outer and inner coil surfaces. Protection heaters were made of stainless steel with 6.2-6.7 Ω resistance at room temperature.

Figure 3.2: LQS01b protection heaters

The 16 protection heaters were connected in 4 groups, electrically separated. Each group contains one heater from each coil: heaters inside the group are on the same coil layer and on the same coil side and are connected in parallel.

The LQS01b protection heaters are made of stainless steel strip. The dimensions of this strip define the resistance R_H of the protection heaters. The voltage V_H has to remain low in order to avoid coil to heater shorts. For this design it is $V_{Hmax} = 450V$. An other important parameter is the power density P_H deposited in the heater. A typical target value is $P_H = 50W/cm^2$.

Due to the length of the coil, half-length protections heaters were used. Therefore each layer has two 1.7 m traces going from the center of the magnet to each end.

A special design was developed because it was impossible to obtain 100% coil coverage, to maintain V_H lower than 500 V and to have power deposition of $50W/cm^2$. The special design consists in a stainless steel strip which is locally narrowed in cross section in order to increase locally the resistance ($R = \rho\frac{l}{S}$ where l is the length and S the section). This design created the so-called "heating stations" equidistantly distributed longitudinally along the coil. Between two heating stations the stainless steel strip becomes wider, providing less Joule heating. Therefore the quenching of the underlying coil area depends on the propagation velocity of the quench generated under the heating stations.

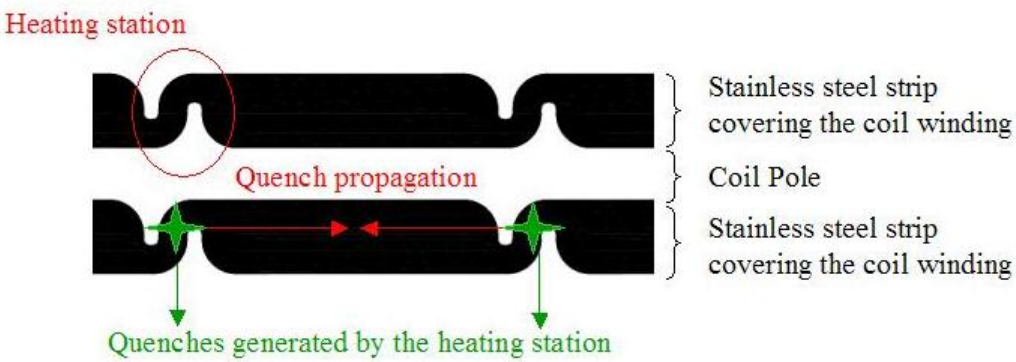

Figure 3.3: Protection heaters design

When quench is detected, the objective of the quench heaters is to quench the whole magnet as fast as possible in order to avoid excessive temperature peak where the quench started. Therefore there are two important parameters for the description of protection heaters:

- t_{Hdelay}: is the "heater delay time" which is the time from when the heaters are fired to the time when the quench induced by the heaters starts ($\sim 12ms$ not more). In LQS01 for maintaining the magnet at a temperature below 350K).
- v_{quench}: is the "quench propagation velocity", needed to quench the coil between two heating stations.

3.2.4 Protection with dump resistor

The external resistors ("dumps resistors") used at VMTF are made of 304 stainless steel and the range of resistance is from 10 to 120 mOhm. In LQS01b is using 60 mOhm dump resistance for allowing the extraction of about 1/3 of the energy.

Figure 3.4: VMTF dump resistor [14]

3.3 Quench History

[2]The results of the first test cycle (TC1) are illustrated in Figure 3.5:

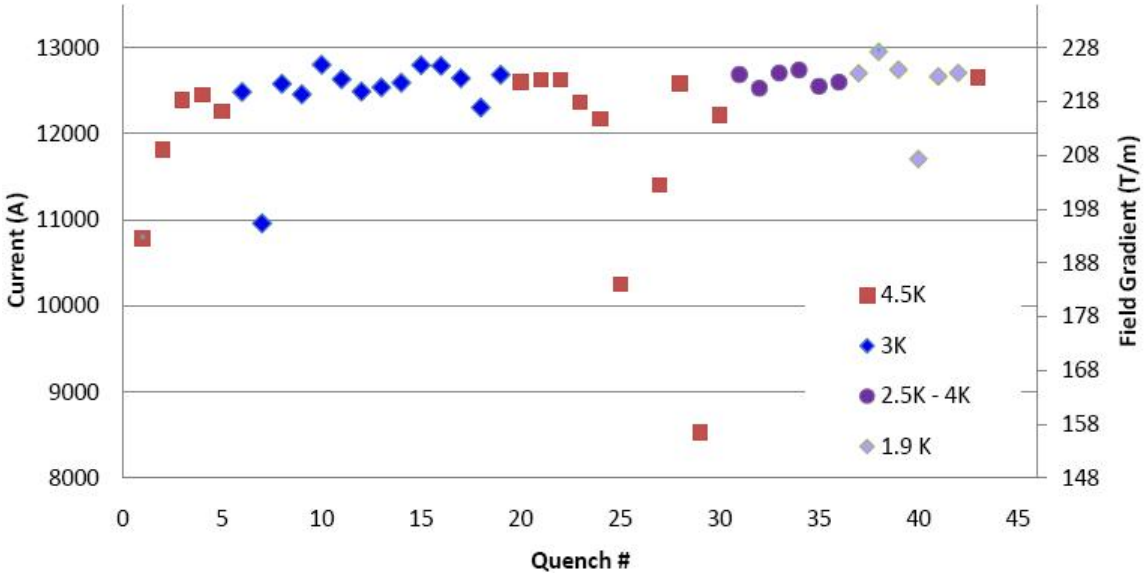

Figure 3.5: LQS01b quench history in TC1

TC1 started with quench training at 4.5K using a variable current ramp rate: 200 A/s up to 3000 A, then 50 A/s up to 5000 A, 20 A/s up to 9000 A and 10 A/s until the quench. Coils #6, #7 and #8 participated in the training at 4.5K.

After a more training at 3 K, the magnet showed a plateau of 222 T/m (12.63 kA) at 4.5 K with all quenches starting in coil #8 outer layer pole turn. Then we did measurement with high

[2]This Section refers to [11]

current ramp-rate (whose study is beyond this work) at 4.5 K, followed by measurements at lower temperatures and at superfluid helium. At 1.9 K only one quench developed in coil #6 inner layer pole turn, whereas all others quenches started in coil #9 from different segments (pole turn of inner or outer layer, or inner layer multi-turn mid-plane block). The last quench in TC1 at 4.5 K was consistent with the previously reached plateau at 222 T/m (12.6 kA).

At the end of the TC1 LQS01b was warmed up to room temperature (the lowest temperature of the magnet was above 270 K) and then was cooled down again to 4.5 K.

LQS01b showed good training memory after thermal cycle and practically in the second ramp the magnet reached the previous quench plateau at 4.5 K.

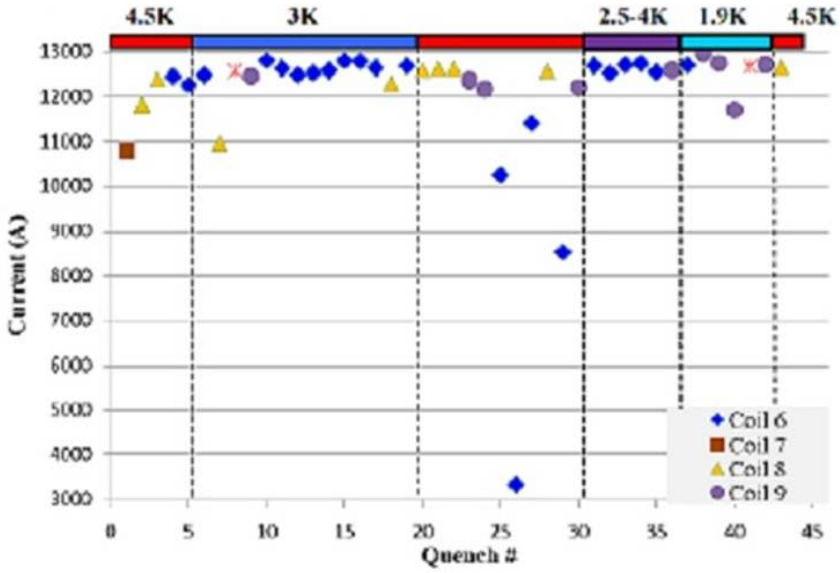

Figure 3.6: LQS01b quench history in first TC with quench locations. Colored bars are used to indicate test temperature.

In total 48 quenches were performed excluding few trips (activation of quench protection system caused by spurious signals) at low current and provoked quenches.

3.4 Quench simulations: QuenchPro

The simulation code QuenchPro [12] is written in the form of a ©Mathcad spreadsheet and is divided into two parts. The first part, which we will use for our study, is for calculation of temperature and current decay; the second part is about the calculation of voltage distribution (we didn't study this part of the program).

Before starting the description it is important to define the time notations used in QuenchPro.

The following plot shows the relevant time notations on a time scale:

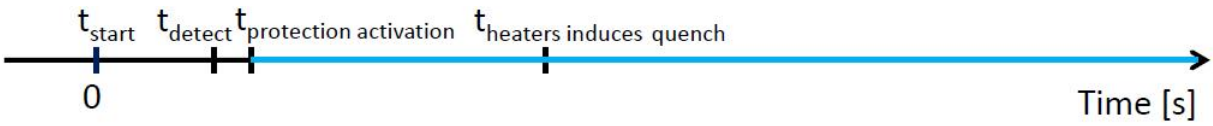

Figure 3.7: Scale of time of QuenchPro

Where:

- t_{start} is the time when quench starts
- t_{detect} is the time when the detection system detects the quench
- $t_{protection\,activation}$ is the time when the dump switch is opened and the heaters are fired; so this is the time when we start the quench protection
- $t_{heaters\,induces\,quench}$ is the time of heat diffusion from heaters into the superconductor until critic temperature is reached
- $\tau_{protection\,delay} = t_{protection\,activation} - t_{detect}$
- $\tau_{heaters\,delay} = t_{heaters\,induces\,quench} - t_{protection\,activation}$

QuenchPro starts the simulations at time: $t = t_{detect} + \tau_{protection\,delay}$ because from t_{start} to $t_{protection\,activation}$ the current in the magnet is constant.

We start the presentation of the program with a description of how the program calculates the main parameters: the maximal temperature, the calculation of the resistance and the calculation of current decay.

- Calculation of Maximal Temperature

In the adiabatic (i.e. without external cooling) approximation the maximal temperature of a quench in a superconductor can be calculated with the formula of the quench integral QI see in 1.11. The QI vs. Temperature is calculated from the material properties (heat capacity, c_p and matrix resistivity). Then the QI is directly calculated from the current decay profile to find the T_{max} given by that specific current decay.

QuenchPro calculates the current decay profile during the quench process. The current I is assumed constant (neglecting the small resistance due to the spontaneous quench) until the quench is detected and the protection activated; from this moment current has an exponential decay (with time constant $\tau = \frac{L}{R_{dump}}$). $t_{heaters\,induces\,quench}$ is the sum of quench detection time t_{detect} and the characteristic time it takes the heat to diffuse from the heater to the coil $\tau_{heaters\,delay}$.

For convenience, the QI is scaled with 10^{-6} to the so called MIITs unit.

- Calculation of the Resistance

The temperature and the magnetic field provide the basis for the calculation of the ohmic resistance.

But, the resistance of each spatial magnet segment is not determined only by these parameters, but also by the length of the normal zone in the segment. For the calculation of the normal zone in the segment, we need information about the nature of quench (spontaneous, heaters induced or through quench propagation), the time when quench occurs and the material properties related to quench propagation (quench propagation velocity, transverse turn to turn heat diffusion time).

- Calculation of the Current Decay

After quench is detected, the time constant τ_i at time i, is calculated from the ratio of the total magnet inductance and the sum of the all resistances in the circuit: $\tau_i = \frac{L}{R_q + R_d}$ where R_q is resistance due to the quench and R_d is resistance of the dump resistor. The time constant is needed for calculating the current decay, and from it the QI, the new temperature distribution in the coils, until the current has dropped to zero.

All this parameters are continuously updated at every new time step of the program: $\triangle t = 5 \cdot 10^{-4} s$.

3.4.1 Input Parameters

3.4.1.1 Material Properties

The material properties that we need for QI calculation are: specific heat, matrix resistivity and geometrical data.

- Specific heat c_p.
- Copper matrix resistivity: it depends on RRR, temperature and magnetic field.
- Geometrical data.

We also need for computing the quench propagation velocity: $B_{c2}(0)$, $T_c(0)$ and Lubell exponent n.

3.4.1.2 Magnet operational parameters

The magnet operational parameters are: magnet length, bath temperature T_b, total inductance L, magnet current I and conductor data (like Copper to Superconductor ratio and total cross-sectional surface A).

3.4.1.3 Quench Protection System Parameters

The heaters distribution array is defined together with the conductor parameters. Quench location and heaters distribution are visualized in the magnet cross-section plot for a better control of the input procedure.

Other input parameters are $t_{protection\,activation}$, $\tau_{heater\,delay}$, $t_{detection}$, and protection dump resistance R_d.

3.4.2 Output Parameters

The output parameters are:

- Plot of Temperature vs MIITs

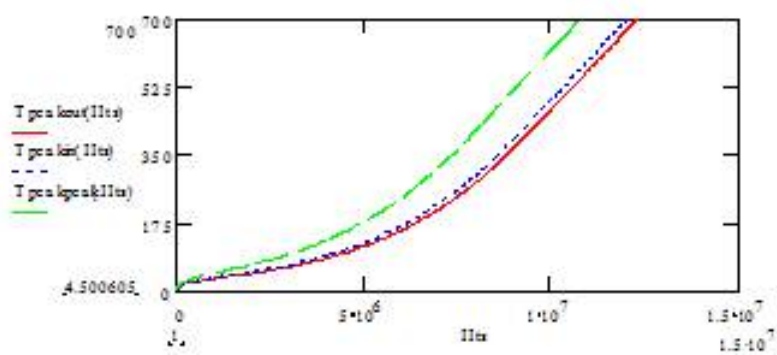

Figure 3.8: Plot T vs MIITs

- Current decay

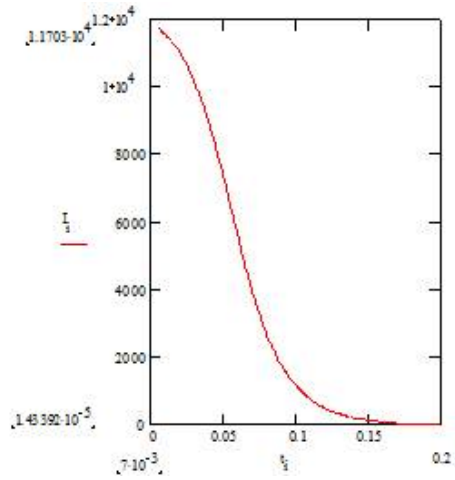

Figure 3.9: Plot current decay

- MIITs at Hot Spot (the point in the coil where the spontaneous quench started)

3.4.3 Program lay-out

The lay-out of the program is outlined in the block-diagram on Figure 3.10:

The code subdivides the coils into segment of half turn. Each half turn is indexed by k, with k=1,2...N, so that many quantities in the program are vectors with N-dimensions. For example the vector that say if the k-th half turn is quenched or not, its quench time, its resistance and many other parameters.

After the input reading, the program calculates the normal zone length. Important derivatives of the normal zone calculation are the quench vector (stating which half turns have and haven't quenched) and the quench time vector (assigning a quench time to each quenched half turn). When the quench induced by the heaters starts the normal zone calculation routine changes in order to take into account also the propagation under the heaters. Maximum temperature, resistance in each half turn is calculated from the normal zone length vector and the quench time vector. The current is recalculated from the updated decay time constant and this procedure is reiterated until the current has completely decayed. The matrix resistivity is recalculated at each time step to account for the temperature change.

The Normal Zone Length:

The time evolution of the quench process is calculated in 2 steps: firstly there is only the propagation of the spontaneous quench secondly there is the additional propagation of the quench induced by the quench heaters after $t_{heaters\,induces\,quench}$.

- Spread of the spontaneous quench $t < t_{heaters\,induces\,quench}$

At $t = t_{start}$ the spontaneous quench starts propagating; the quench will propagate with the predefined quench propagation velocity along the conductor up to the end of the turn.

- Spread of the heater action at $t_{heaters\,induces\,quench}$

At $t_{heaters\,induces\,quench}$ turns covered by the heaters are quenched over their full length or partially depending on the heater design. The quench under the heaters propagates with a predefined velocity different from the velocity of the spontaneous quench (which is usually faster being in a high field zone).

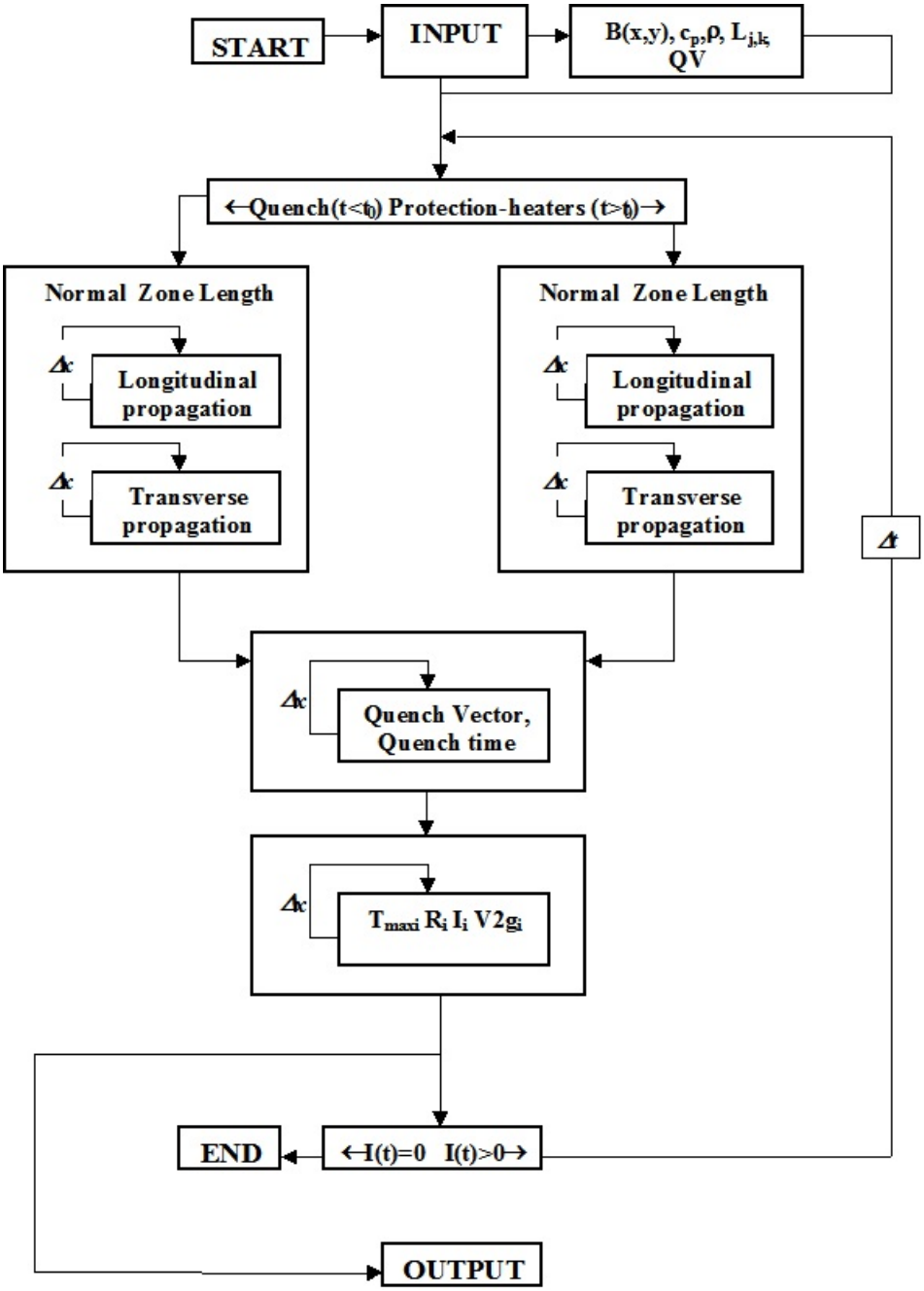

Figure 3.10: QuenchPro block-diagram

The Temperature Growth :

The temperature T_k growth is calculated from the quench-integral at each given time. The quench integral has to be recalculated with each time step $\triangle t$ $(t_i = 0 + \triangle t \cdot i)$, with i the time index, according to:

$$QI_{i+1} = QI_i + \triangle t \, (I_i)^2$$

The quench vector allows to assign the correct value of QI to each half-turn. In the segment that experiences a spontaneous quench at t=0 the QI computation starts at t=0; whereas in the segments covered by a heaters the QI computation starts at $t_{heaters\,induces\,quench}$.

The Resistance :

The resistance of half turn k r_k is given by $r_k = \rho_{Cu}\left(B_k, T_k\right)\frac{xq_k}{A_{Cu}}$ where ρ_{cu} is the resistivity of the copper in function of the magnetic field, RRR and the temperature, xq_k is the normal zone length and A_{Cu} is the copper cross section.

In order to be conservative, the temperature used in the resistivity computation is the maximum temperature of the k-th half-turn calculated according to the procedure presented above.

The total resistance of the electric circuit at time t_i is the sum of the resistance of all half turn plus the dump resistance:

$$R_i = R_d + \sum r_{k,i}$$

The current :

The time constant at time τ_{i+1} for calculation of the current decay, is computed from the magnet inductance and the total resistance R_i.

$$\tau_{i+1} = \frac{L_{tot}}{R_i} \tag{3.1}$$

The calculation of the current decay is (in the approximation of $\frac{\triangle t}{\tau_i} << 1$, $\triangle t = 5 \cdot 10^{-4}\,s$, $\tau_i = 0.18\,s$):

$$I_{i+1} = I_i\left(1 - \frac{\triangle t}{\tau_i}\right)$$

Further details about QuenchPro can be found in [12]. We have modified a few parameters for better simulating the design of the Long Quadrupole.

The first modification that we have introduced into the program allows using Heating Stations in the quench vector (in the formula of the Resistance R_{i+1}): in the LQ magnet there are 28 HS with a separation between stations of 11 cm. The quench induced by the heaters propagates in two directions, on the left and on the right of the normal zone therefore the propagation velocity was multiplied by the number of heating stations in order to simulate the normal zone growth caused by the heating stations.

An other significant modification regarded the inductance L and the computation of the time constant. We will explain the reason for this change in Chapter 5. In the original QuenchPro L is a constant used in the computation of the time constant in Equation 3.1. We modified this part of the code by introducing loop *if* over the current value and by associating to different current ranges different values of the inductance. Therefore L does not remain constant during the current decay, but changes with the current.

3.5 Quench simulation: QLASA

In order to obtain more precision for the simulations of the current decay, we decided to use QLASA [13] which is a computer code for quench simulation in adiabatic multicoil superconducting windings.

The flow-chart of the computer code QLASA is reported in Figure 3.11.

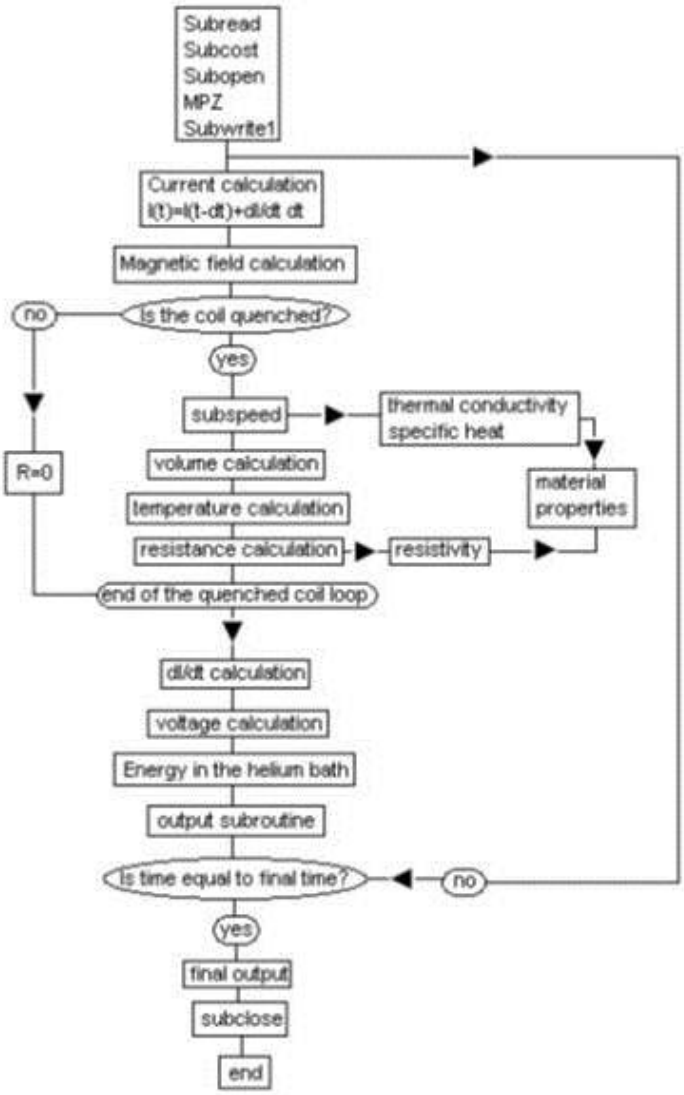

Figure 3.11: Flow-chart of the computer code QLASA

Input parameters are:

- Number and geometric dimensions of the wining
- Time and position of the quench starting point
- Operating current, critical current of the cable and magnet field locations
- Self and mutual inductances
- Cable components and their percentage in the unit cell
- Information about electric circuit: dump resistance, delay time, arc time, number of magnets electrically connected in series.

The quench propagation velocities are computed according to the theory reported by M.N.Wilson [1]. We will not enter in a detailed description of the program. However it is interesting to explain how we adjusted QLASA for the topology of accelerator magnets.

The goal is transforming a volume of a quadrupole ($cos\,2\theta$) in an equivalent volume for solenoid.

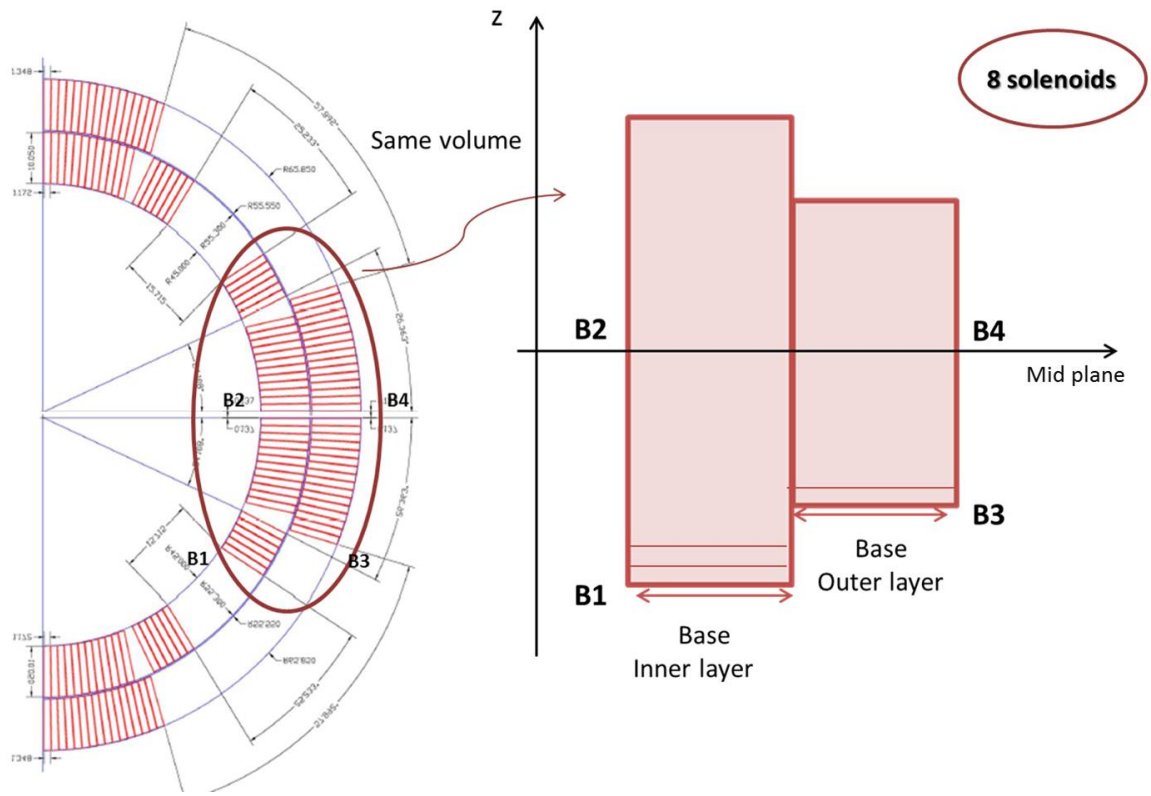

Figure 3.12: Transformation of a $cos\,2\theta$ quadrupole (whose cross section in shown at left and whose coils are straight with a length L) in an equivalent volume solenoid (whose cross section is shown at right, for only one 1/2 of the coil)

In order to respect the as more as possible the geometry of the quadrupole, we decided to map the inner and outer layer into two independent solenoids with the same current. The choice of separate inner from outer layer allows a better representation of the protection heaters which in LQS01b are installed on both the outer and inner coil surfaces. With this procedure we obtain in total eight solenoids representing the four inner layers and the four outer layers.

Each inner layer of the quadrupole coils has 36 turns while each outer layer has 32 turns. In 3.12 there is also the correspondence of the magnetic field points of the quadrupole and of the solenoids. B1, B2, B3 and B4 are the necessary input parameters of the QLASA program.

For obtain the same volume between the quadrupole and the solenoid we impose:

- $Base_{\,cos\,2\theta} = Base_{\,Solenoid}$.
- $Height_{cos\,2\theta/inner\,layer} = Height_{Solenoid} = 36 \cdot thickness$.
- $Height_{cos\,2\theta/outer\,layer} = Height_{Solenoid} = 32 \cdot thickness$.

In QLASA the quench starts and propagates naturally in one solenoid, while in the other solenoids it is induced by quench heaters.We also used two coefficients for the correction of the velocities of propagation of the quench:

- *corvz* is for the longitudinal velocity; since we have 28 heating stations (or heating points), the longitudinal velocity is multiplying by setting $corvz = 28$.
- *corvre* is for the radial velocity toward outer radius; since we have a single flat cable, the homogenization treatment of the unit cell done by QLASA is underestimating the actual radial speed, because in reality the heat does not need to diffuse throughout the radial insulation. Therefore this effect has been corrected by setting $corvre = 15$.

Chapter 4

The experiment

4.1 Introduction

The goal of a study described in this chapter is to provide a comparison between the experimental data and simulation performed with the standard QuenchPro package [12]. The input parameters were selected and settings of the QuenchPro simulation code were optimized to achieve a better agreement with the test data. This study eventually will help to improve quench simulations for future magnets designed within the High Luminosity Upgrade program at the Large Hadron Collider (CERN). The experimental data were collected at Fermilab during the test of LQS01b, the first Nb_3Sn long quadrupole magnet made by LARP. This 4 m long and 90 mm aperture magnet was assembled in an Aluminum-shell based structure. Test was performed at the Fermilab's vertical magnet test facility (VMTF).

4.2 Test facility for superconducting accelerator magnets

4.2.1 Test facility

Nb_3Sn magnets at Fermilab are tested in the Vertical Magnet Test Facility capable of efficient operation at a superfluid liquid helium temperature. Most of tests in the VMTF are performed between 1.9 and 4.5 K. One of the major components of the test facility is the dewar, designed for magnets up to 4-m length and 0.62 m diameter. Figure 4.1 shows a cross section of the VMTF.

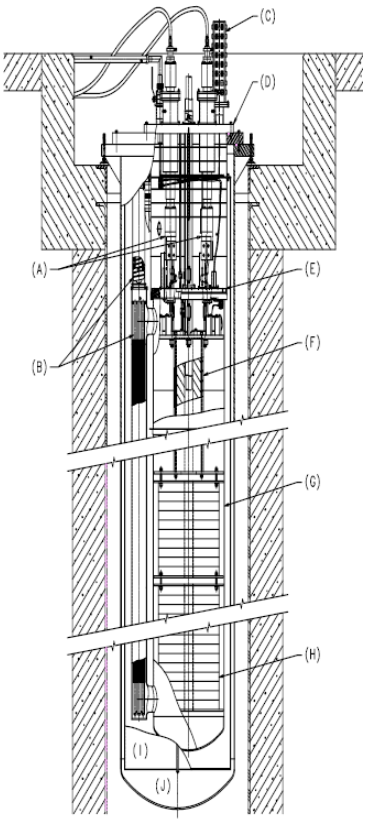

Figure 4.1: Cross section of the VMTF [15]

Legend:
(A): Vapor cooled leads
(B): Heat exchanger
(C): Instrument tree
(D): Top Plate
(F): Magnet
(G): Helium Shell
(H): Displacer
(I): 80K Shield
(J): Vacuum shell

The helium shell in the dewar is separated from the outer vessel by a vacuum space and insulation, and with an 80 K shield. The cryostat top flange is equipped with a liquid helium inlet and outlet pipes. Recently helium recovery line was added to the test facility in order to reduce helium consumption, especially for magnets with a large stored energy. The top flange is also equipped with power leads rated for currents up to 30 kA. These current leads are connected to a 30 kA-30 V D.C high precision power supply through the water cooled flexible power leads. Inside the dewar, the vapor cooled leads are connected to a large 17 mm wide Nb-Ti superconducting cable, which usually are soldered to the magnet leads. The helium volume in the cryostat is divided in two parts by an insulator plate, so called lambda plate. The upper bath contains liquid and vapor helium at 4.2-4.6 K, and the lower bath, which can be either isothermal to the upper bath or can be separately cooled down, contains liquid helium at 1.8-4.6 K. The temperature in the lower bath is controlled by a built-in heat exchanger. The heat exchanger consists of 4 m long copper tubes in

direct contact with the helium in the lower bath. Vacuum pumps are capable removing more than 30 W of heat at 1.8 K. There are several penetrations through the lambda plate for the magnet and dewar instrumentation, superconducting power leads to feed the magnet and for pressure relief valves. The test facility is equipped with a helium liquefier capable to produce ~250 liter per hour of liquid helium at 4.2 K. The cryogenic system is completed with the liquid helium distribution lines, providing the cooling fluid to the various testing stations, and with the return lines to recover the helium gas and put it again through the liquefier. The magnet is vertically suspended with rods to the lambda plate, which itself is suspended to the cryostat top flange. The magnet is fully immersed in a liquid helium bath whose level change is continuously monitored in order to keep it at the optimal level. The liquid level should be high enough to cover the welded copper to NbTi joint at the copper power leads and below the holes in the copper power leads for the cooling vapor flow. The helium volume can be significantly reduced for small magnets by using foam displacers. Another major part of test facility is a 30000 A, 30 V DC power system. The power system for VMTF is based on six commercial 150 kW Power Energy Industries (PEI) power supply modules, 30 kA/1kV dump resistor and two 15 kA/1kV DC solid-state dump switches. Additional in-house electronic components were designed and built to provide precise current regulation and distribution. The PEI power supply modules are connected in a master/slave configuration. The Master Power Supply provides the Silicon Controlled Rectifiers (SCR) firing signals for all modules. Each power supply has four firing modules with three SCRs each (one per phase), for a total of 12 SCRs. Current regulation is accomplished by an external precise current regulator cascaded to the Master Power Supply's internal regulator set to "Voltage" mode. Each PEI supply is capable of delivering 5,000 Amps DC at 30 Volts. There is also the option of tapping the supply at higher voltages with the corresponding decrease in maximum current. The system is highly modular, and it can operate with just the master supply or with the master supply plus any combination of slave supplies.

At the VMTF, the stored energy extraction from a magnet is accomplished by quickly switching a load resistor in series with the bus. Fast switching is accomplished with two 15 kA 1000 V DC solid state dump switches. These switches include six SCRs mounted in water-cooled heat-sinks. The SCRs continuously carry their share of the rated current, and they are commutated off from stored energy in capacitors. Once the SCRs turn off, the bus current flows through the dump resistor connected in parallel with the dump switches. The switch opening time is approximately 25 us after detection of a fault or a trip command. The dump resistor dissipates the stored energy from the magnet after a quench or trip. The dump resistor at VMTF built from air-cooled stainless steel elements, is rated for a maximum current of 30 kA, a maximum energy dump of 3 MJ, and a maximum voltage across the resistor of 1000 V dc.

Quench detection system at VMTF includes three subsystems: an Analog Quench Detection (AQD) system based on VME modules, a Digital Quench Detection (DQD) system and a FPGA-based system. These systems work in parallel for redundancy. The FPGA-based quench detection system was developed recently to set a current dependent threshold for the quench signal. Quench detection threshold can be set in 10 different current regions. The current dependent threshold proved to be very useful for magnets with large transient magnetic flux changes in the conductor. These flux changes can produce voltage spikes of the order of 1-2 V. These spikes, mostly observed at magnet currents up to 5-6 kA, can easily trigger a quench detection system. The new detection system has a current dependent threshold allowing high threshold at low currents, to avoid trips due to the voltage spikes, and low threshold at high magnet currents, to maintain peak temperatures below the upper limit (350-380 K). A Fermilab built VME Quench Logic Module (QLM) monitors the quench status and sets off a chain of events that controls the phase off of the power supply, the energy extraction circuit firing, and the magnet quench protection heater discharge. The Quench Management Software manages the operation of the Quench Management Hardware and its iterations with external components such as the quench characterization hardware, which is used for capturing and characterizing magnet instrumentation data, and the quench protection heaters. It also provides user settable parameters via a graphical user interface GUI.

The data acquisition system is very sophisticated allowing data sampling at a frequency of 10 kHz. All the data are eventually stored in a computer file. The voltage spike detection system (VSDS) based on a National Instruments PXI multifunction DAQ was developed at Fermilab for detection of a small magnetic flux changes (thermo-magnetic instabilities, flux jumps) in superconducting magnets. The VSDS captures half-coil signals at a sampling rate of 100 kHz.

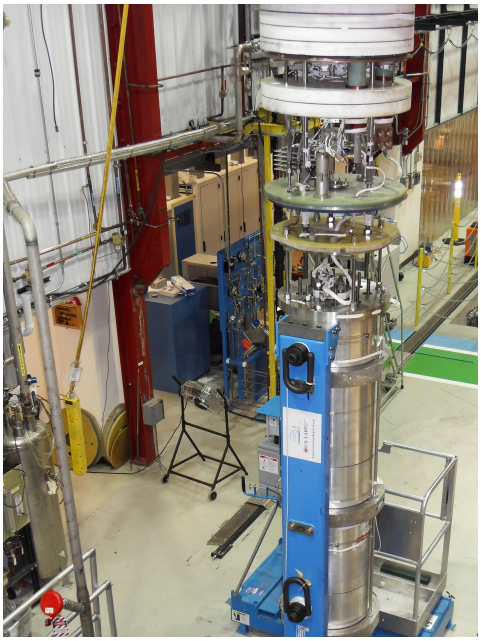

Figure 4.2: Photo of the test facility from the top [14]

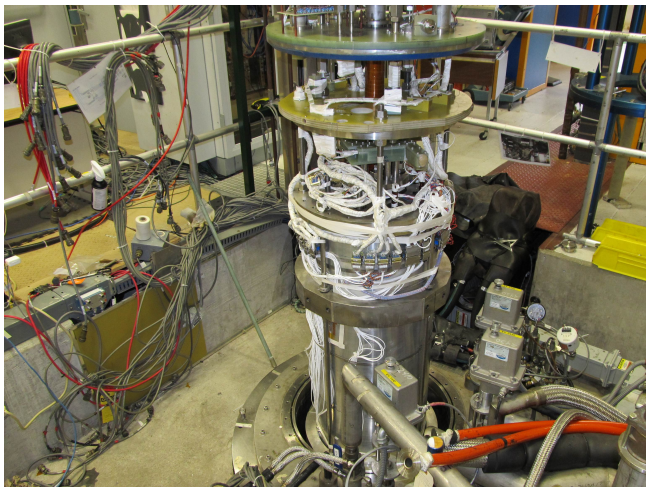

Figure 4.3: Magnet before enter in the vertical dewar [14]

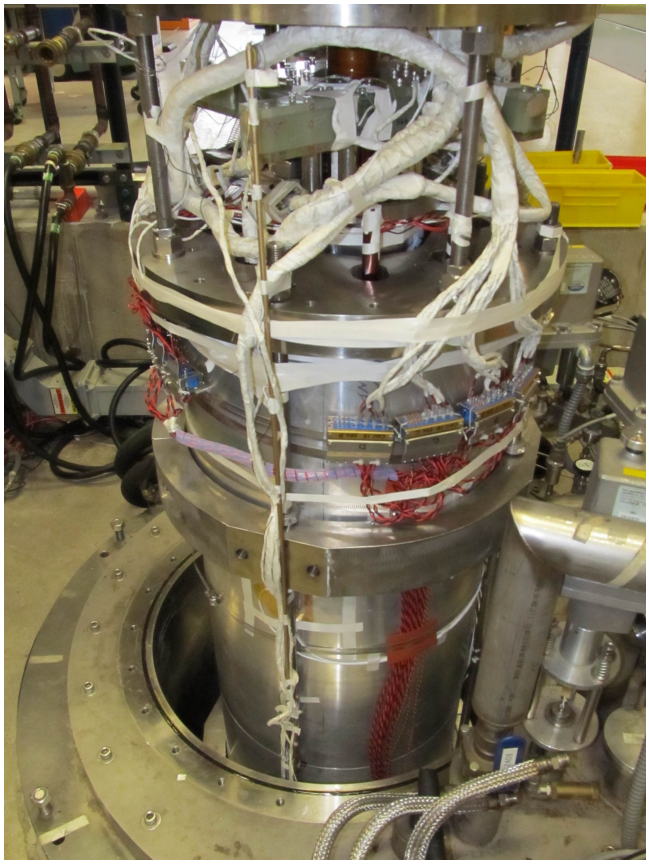

Figure 4.4: Magnet before enter in the vertical dewar [14]

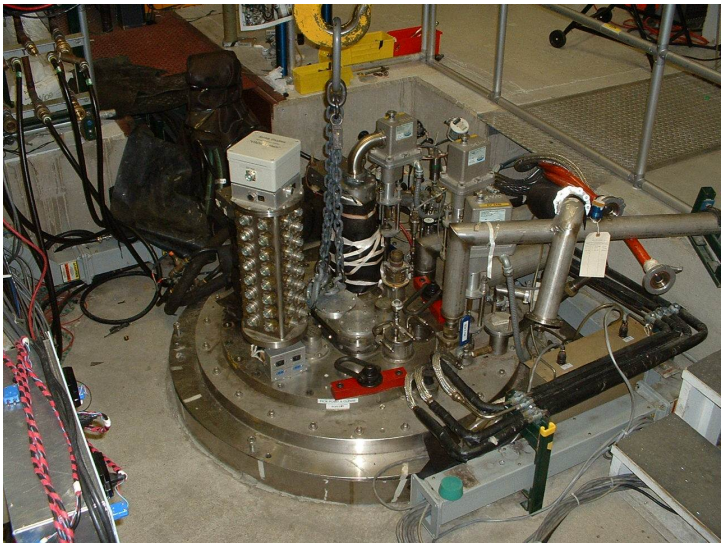

Figure 4.5: Magnet in the vertical dewar [14]

4.2.2 Quench test procedure

Superconducting magnet test procedure includes room-temperature preparation, electrical check-out at 4.5 K, quench training, ramp rate dependence study, field quality measurements and other tests at 4.5 K or lower temperatures and post-test electrical check-out. Comprehensive electrical check-out of all magnet instrumentation usually is performed before the magnet cool down starts. Test of the electrical integrity of the magnet is an essential part of test preparation. Hi-potential (hipot) test of coils to ground or heaters to coil and ground is very important to verify that the coil and heater insulation is sufficient for the safe operation of magnet at high currents. Hipot test usually is performed before and after the cool down. Cool down of LQS magnet takes about a week because of the restriction that temperature difference between any two points of the magnet should not exceed 100 K. Temperature change at the magnet top and bottom is shown in Figure 4.6. Mechanical behavior during cool-down and warm-up is monitored with the set of strain gauges mounted on support structure components and coils.

Figure 4.6: LQS magnet cool down

Field quality is of great importance for to the accelerator magnets because it affects beam optics and stability of the beam. Magnetic measurements are performed at room temperature, as well as before and after the quench training at 4.5 K. Quench training starts at 4.5 K with ramps at a rate of 20 A/s. The magnet current is increased continuously until a quench happens. The Quench Management (QM) system initiates the magnet protection system, disconnects the power supply and dumps the stored energy through the extraction circuit after the quench is detected. The extraction circuit protects the superconducting accelerator magnet after a quench. Without an extraction circuit, after a quench, practically the whole energy of the system would be dissipated in the magnet normal zones, heating the coil and generating huge turn-to-turn and coil to ground voltages. Even if the power supply stops supplying energy into the system, the energy stored in the magnet could be enough to damage the cable. Indeed, since the propagation velocity of the normal zone is usually low relative to the heating rate, the energy would be dissipated in a small region which could reach temperature values harmful to the coil materials. Dump resistor of 60 mOhm was used for LQS magnet tests with the expected maximum voltage ($I_{max} \cdot R_{dump}$) of about 800-900 V. LQS coils can see only half of this voltage because of the symmetric magnet grounding at VMTF. Quench training at 4.5 K usually continues until the quench plateau is reached. After ramp-rate dependence study the magnet is cooled down to a lower temperature. Part of LQS magnet training was done at 3 K instead of 4.5 K in order to reduce helium consumption during the test. Later on

the quench performance is tested at 1.9 K. LQS01b quench training is shown in Figure 3.5.

In our magnet the current density J_c is very high and because more or less the copper cross section is the same as the cross section of superconductor (for Nb_3Sn we consider the bronze and the barrier as part of the SC), also J_{Cu} is very high, $2000 - 2500\ A/mm^2$; therefore, the hot spot temperature given by equation 1.7 valid in adiabatic approximation, can be dangerously high. We want to avoid high temperature peak for minimize risk of damaging the magnet: since J_{Cu} is very high, the resistivity is more or less fixed, the time dt must be very short. This implies a very fast protection activation and a fast extraction of the energy. A high hot spot temperature can cause magnet detraining during the same cycle, i.e. a subsequent training happens at a current level lower that the previous one, because of thermal stresses.

The experimental data of the different ramp of LQS01b that I've analyzed during my work was taken during a cold test at Test Facility.

The parameters that we note in the book of a Summary Test are: Date, Ramp #, Quench #, Current [A], Gradient [T/m], Final Ramp [A/s], Temperature [K], MIITs when quench is detected, $t_{detection}$ [s], Coil, 1st segment, 2nd segment and 3th segment.

The datas that I've analyzed are presented on Microsoft Excel in two columns: time (from -1s to 1s) and current I.

For more precision about times notation in Data file's used I have made a simple graphic:

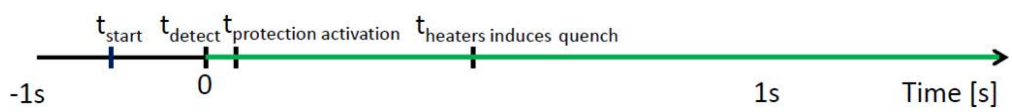

Figure 4.7: Experimental times notations

where times notations used are the same used in 3.4.

We can observe that time notation in QuenchPro is different from time notation in experimental data; so, in order to have the same time notation, in our work we have chosen experimental time notation i.e. t= 0 is the detection time.

Chapter 5

Data analysis

5.1 First comparisons between experimental and simulation data

After becoming aware of the impact of each input parameters in QuenchPro: RRR, $t_{heaters\ induces\ quench}$, magnetic field, etc.. we started a comparison of the experimental current decay with simulations results given by QuenchPro.

We summarize in the following Table 5.1 the input used in QuenchPro for RAMP #4 (we did this study for many ramps #):

Table 5.1: QuenchPro inputs for Ramp #4

I [A]	12454
T [K]	4.54
l [m]	3.6
$\mathbf{B_{in}}$ **[T]**	2
$\mathbf{B_{out}}$ **[T]**	1
$\mathbf{B_{peak}}$ **[T]**	11
RRR	100
$\mathbf{v_{qin}}$ **[m/s]**	40
$\mathbf{v_{qout}}$ **[m/s]**	10
L [mH]	13
$\mathbf{R_{dump}}$ **[mΩ]**	60.5
$\mathbf{t_{qdet}}$ **[ms]**	-5.4
$\tau_{\mathbf{heaters\ delay}}$ **[ms]**	5
$\mathbf{t_{protection\ activation}}$ **[ms]**	1

where B_{in} and B_{out} are respectively the average magnetic field in inner layer and in outer layer and B_{peak} is the magnetic field where quench starts. The values of B_{in} and B_{out} are chosen for be conservative in the computation of MIITs and the temperature because with low magnetic fields there is less effect of the magnetoresistance, therefore less increase of the resistance in the coil. v_{qin} and v_{qout} are the respectively velocity of the quench in the inner and outer layer. Quench velocity in the inner layer derived from measurements on other magnets and quench velocity in the outer layer is a conservative value.

And the plot obtained is reported in Figure 5.1.

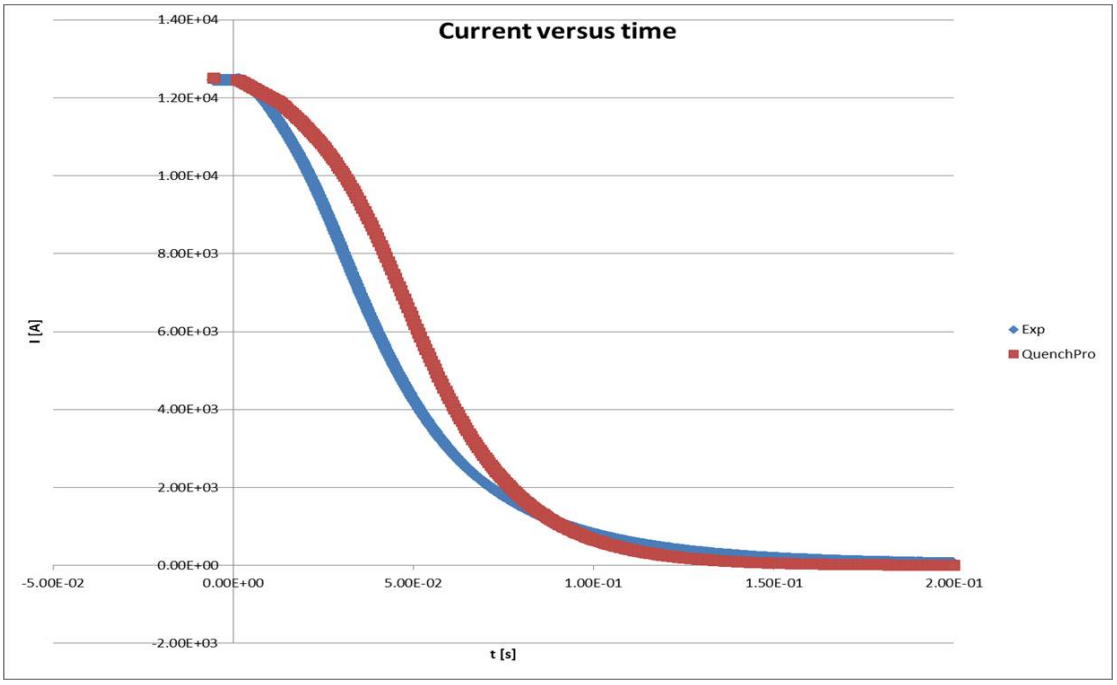

Figure 5.1: Ramp #4

We can observe that the two currents decay have different slopes. Therefore first of all, we focused on the first part of the plot, before $t_{heaters\ induces\ quench} = 6\ ms$, in order to understand why there is a discrepancy since the beginning. It's important to obtain in this time range a good approximation between experimental data and simulation because this is the first part of the current decay. At the beginning, when quench is detected (t=0 in the plot) before $t_{heaters\ induces\ quench}$ the law of current decay is $y = a \cdot \exp\left(-\frac{t}{\tau}\right)$ where $\tau = \frac{L}{R}$. The resistance is approximately $R_{dump} \approx 60.5\ m\Omega$ because the heaters are not yet activated, and the coil resistance due to the natural quench propagation is negligible with respect to the dump resistance. In the plot of current decay, just at the beginning (i.e. the first milliseconds [1-4.9ms]) we can easily study the time constant τ, while after this range of time there are more parameters which can influence the current decay (the velocity of propagation of the quench, the magnetic field, etc).

The zoom of this first part with timing notation is shown in the Figure 5.2.

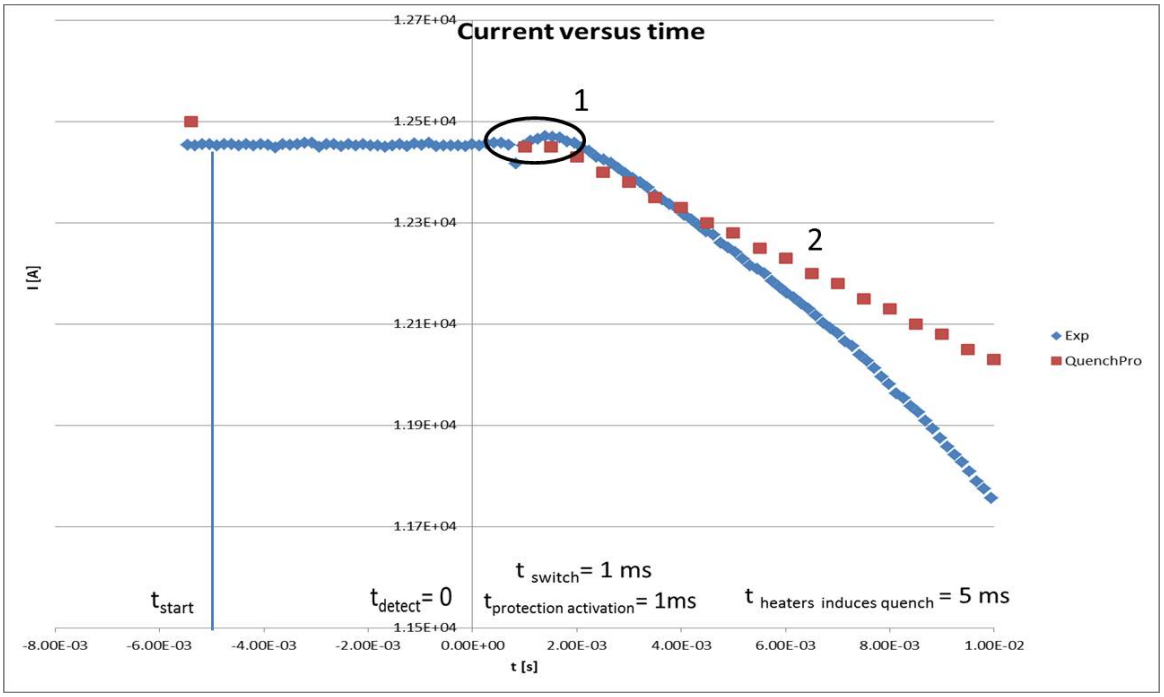

Figure 5.2: Zoom Ramp #4

At the begging of experimental current decay we can observe an initial bump, see circle 1 in the Figure 5.2 : it is caused by the switch opening, which lasts for about 1 ms. Therefore in the next set of simulations (second part of the study) we added 1 ms to the protection activation delay time.

In the 2nd part of the plot, we can see that the experimental current decay decreases faster than the current decay simulated with QuenchPro.

For understanding the reason on this phenomenon, we fitted the experimental current decay in the time range from 1 to 4.9 ms with an exponential trendline. From the fit we infer the time constant τ, and assuming for the inductance L the value computed at room temperature (therefore at low current) before the test, L= 13 mH, we obtained the value of the resistance.

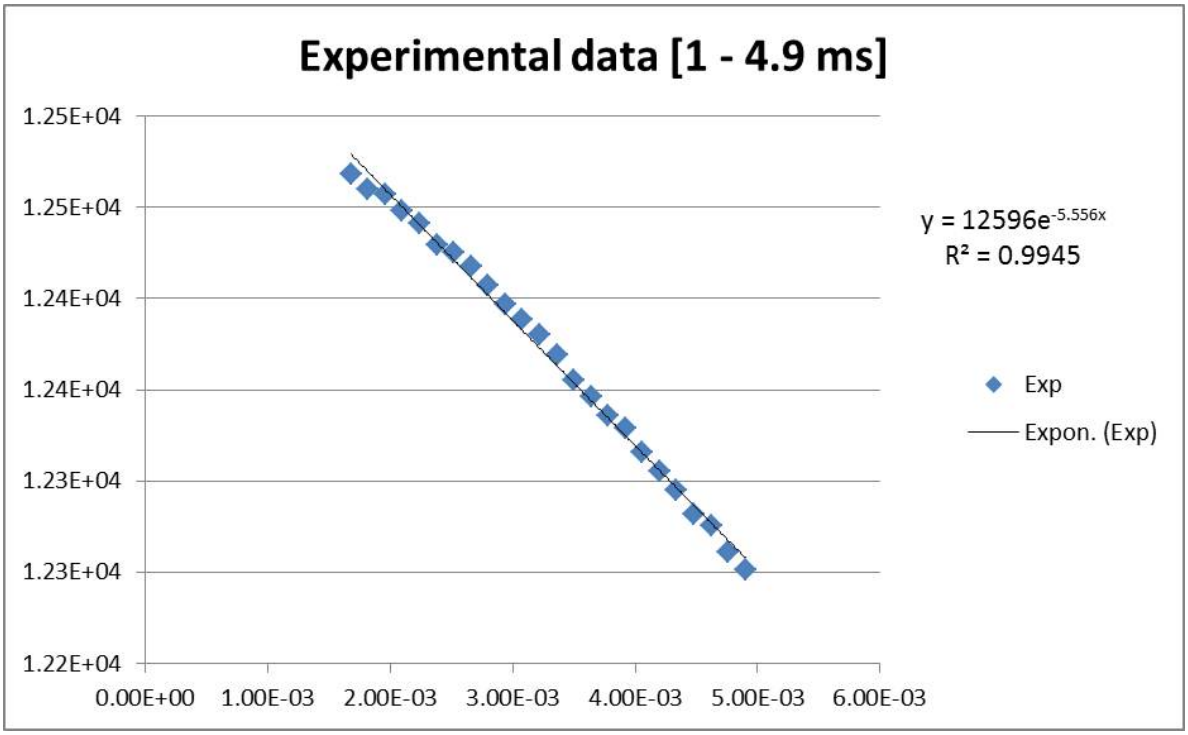

Figure 5.3: Fit of Ramp #4

The equation obtained by the exponential fit is:

$$I = 12596 \cdot \exp\left(-5.556 \cdot t\right) \ [A]$$

where:

$$\frac{1}{\tau} = 5.556 \ \left[s^{-1}\right]$$

So:

$$\tau = 0.179 \ [s]$$

Then the resistance is:

$$\mathbf{R_{tot} = 72.2 \ [m\Omega]}$$

This value of the resistance is very high compared with R_{dump}.

We repeated this study with different Ramps# and at each study we got a value of resistance about 20-25% higher than R_{dump}.

The Table 5.2 is a recap of this analysis:

Table 5.2: Summary table

	Ramp #	**I**	**T**	$\mathbf{t_{detect}}$	**MIITs**	**L**	$\mathbf{R_{tot}}$	τ	**Interpol range**
		[A]	**[K]**	**[ms]**		**[H]**	**[mOhm]**	**[s]**	**[ms]**
Exp	1	10782	4.6	-11.3	5.89	0.013	70	0.19	1-5
QuenchPro					6.23		60	0.21	
Exp	2	11818	4.6	-8.3	5.76	0.013	72	0.18	1-5
QuenchPro					5.88		62		
Exp	4	12454	4.54	-5.4	5.45	0.013	72	0.18	1-5
QuenchPro					5.89		61		
Exp	56	12577	4.56	-5.4	5.54	0.013	74	0.18	1-5
					5.9		62		
Exp	35	6145	4.5			0.013	73	0.18	1-5
Exp							76	0.17	1-10

In the table for each current ramp we put Experimental values and QuenchPro values. We can observe, in Ramp #1, #2, #4 and #56, that the higher is the current the higher is the total resistance R_{tot} obtained by this computation method.

Apparently R increases significantly with the current, and so we made the hypothesis that there is a "quench back" (quench of additional parts of the coil included by the spontaneous quench, but not through standard propagation) which may explain the reason why the resistance at the begging of a quench is so large. We checked this hypothesis by calculating the resistance per meter of quenched cable.

There are L=215 m of cable in a coil, and the cable is made of 27 strands (strand diameter is 0.7 mm) composed of Copper, Nb_3Sn and Bronze.

Figure 5.4: Strand materials

We have calculated the total cross section of the cable S, and obtained the resistance per unit length: $R_l = \rho \frac{S}{l}$ where $l = 1 \cdot \frac{1}{cos\,\theta}$, where this last term takes in account the longer length of the wire inside the cable due to pitch angle of the Rutherford cable and ρ $[\Omega \cdot m]$ is the resistivity of each material. The resistivities are computed by a MATPRO library [16], with RRR= 150 (for copper), B= 11 T and T= 50 K. The temperature was estimated from the MIITs computed a few milliseconds after the quench detection and anyway before heaters could induce the quench; the obtained value was used in QuenchPro which calculated the temperature. Assuming the different materials as parallel electrical resistors, we have that: $\frac{1}{R_l} = \sum \frac{1}{R_n}$. For Ramp #1 we had $R_{TOT} = 70\,m\Omega$ and dividing $(R_{TOT} - R_{dump})/R_l$, the total quenched length is $L = 44.18\,m$. This result was very unexpected because is impossible that at the beginning of the quench the quench back had quenched 44.18 m of cable in very few ms. We decided to check if there is an important magnetic diffusion time which could give a high resistance. Magnetic diffusion time is the time that the current takes to flow form the superconducting filaments into the stabilizing copper. This hypothesis was exclude because we have verified that the magnetic diffusion time constant in our case is very short, $\tau_{Diffusion} \approx 10^{-4} sec$, compare to our time scale (a few ms).

Due to these results we decided to repeat this analysis on Ramp #35, which was a trip of the power supply without quench in the coil. We expected to obtain $R_{TOT} = R_{dump} = 60.5 m\Omega$ because there was no quench development in the coil. As we can see in the Table 5.2, Ramp #35 reached I= 6,145A at T= 4.5 K. Assuming the same value of the inductance previously used (L= 13 mH), we obtained again $R_{TOT} = 73\, m\Omega$ with an interpolation range of [1ms-4.9ms] and $R_{TOT} = 76\, m\Omega$ with an interpolation range of [1ms-10ms]. This result was quite unexpected.

After double checking the resistance of the whole system (dump resistor, current leads and bus bars) the only reasonable conclusion was that the effective inductance during the current ramp down was not L= 13 mH. Since the time constant is $\tau = \frac{L}{R}$ and in Ramp #35 the resistance is $R = 60.5\, m\Omega$ we obtain $L_{effective} = 10.8\, mH$.

This conclusion, valid for Ramp #35, should have an impact also on the other Ramps. However things are more complicated as explained in the next section.

5.2 Second part of the study

In the previous part we discovered that the inductance is not 13 mH, but it changes as a function of the current.

In the second part of the work we investigated the time constant at the beginning of current decay. As we did in the previous section, we made an exponential fit of the current decay in the time range 2-4.9 ms. This is the time range between the full opening of the switch and the earliest start of the effect of the heaters: in this time interval we know that the resistance of the circuit is approximately $R = R_{dump} \approx 60.5\, m\Omega$.

We obtained the following plot showing time constant of several quenches after current ramps with different ramp rates:

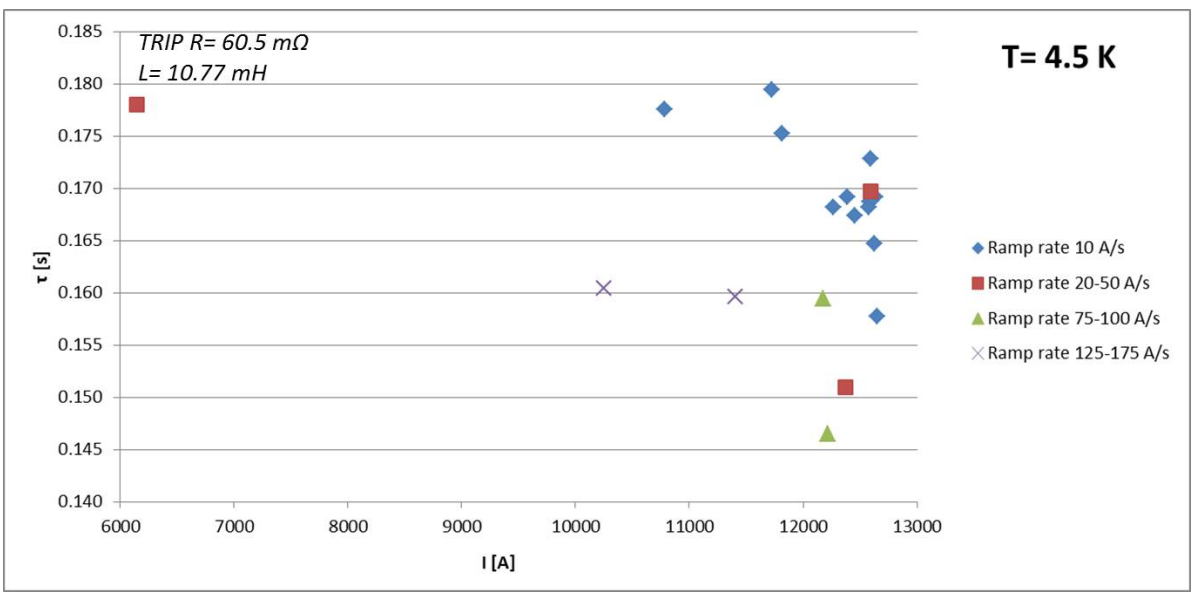

Figure 5.5: Time constant τ versus current I at different ramp rates

We can see that at high ramp rate τ decreases significantly. In the following, we decided to exclude the quenches after the high ramp rates and to focus only on quenches at low ramp rate (10 A/s). In the 5.6 we plot again τ versus current only for the quenches with 10 A/s ramp rate together with the reference point given by the trip at I= 6145 A.

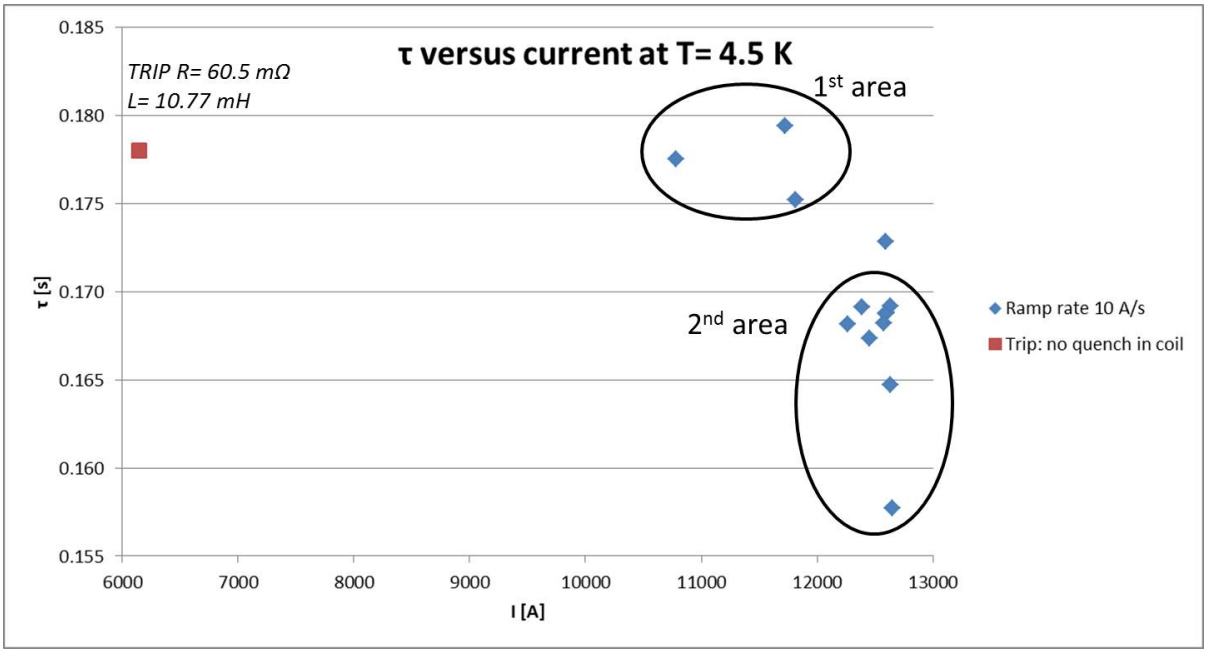

Figure 5.6: Time constant τ versus current I for 10 A/s rate and for the reference trip

The experimental data are basically grouped in two families indicated by the two oval areas: in the 1st area, the value of τ is consistent (within $\pm 1.5\%$) with the one given by trip. However in the 2nd area the time constantτ decreases in average by 5%, a value which is not consistent with the trip. We believe that in this 2nd area a new phenomenon affecting the resistant growth plays an important rule. For the moment we concentrate on the study of the first area to try to understand the actual value of the inductance and later we will tackle the understanding 2nd of the area.

5.2.1 Study of the 1st area

In this part of the plot the time constant τ is very similar to the one computed during the trip, therefore the inductance L in this region is the same as the one computed for the trip.

It should be noted that this value of the inductance is about 17% less than the value measured at low current.

Therefore we decided to make a comparison among the inductance obtained through the experimental data, the measurements at room temperature, and the estimates of the inductance obtained by computing the stored energy.

5.2.1.1 Experimental data

The experimental values for the quenches of the 1st area and the trip are shown is in Table 5.3:

Table 5.3: Experimental data of the 1st area

I [A]	τ [s]	**L [mH]**	**Final ramp rate [A/s]**	
6 145	0.178	10.77	50	TRIP
10 782	0.178	10.74	10	
11 726	0.179	10.85	10	
11 818	0.175	10.60	10	

During the first part of the current decay $R = R_{dump}$ so the value of the inductance is simply given by: $L = \tau \cdot R_{dump}$.

5.2.1.2 Study of the dynamic inductance from the computation of the energy

In the Long Quadrupole magnet the iron is very close to the coils and has a significant impact in the computation of magnet energy and inductance. For this analysis the dynamic inductance $L_{dynamic}$ has to be computed from different values of the stored energy. Using the fundamental law of the electromagnetism, an infinity variation of energy dE:

$$dE = -I \cdot \epsilon \cdot dt = I \cdot d\phi = I \cdot d(L \cdot I) = I \cdot (L \cdot dI + I \cdot dL) \tag{5.1}$$

where ϵ is the voltage at the terminals of the inductor L in which is flowing the current I.

The relation between the static inductance L_{static} (defined as $L = L_{static} = \frac{\phi}{I}$ where ϕ is the magnetic flux) and the dynamic inductance $L_{dynamic}$ (define as $L_{dynamic} = \frac{d\phi}{dI}$) is:

$$L_{dynamic} = L_{static} + \frac{dL_{static}}{dI} \cdot I$$

Then from 5.1 we obtain:

$$\frac{dE}{dI} = I \cdot L_{dynamic}$$

that can be written as:

$$L_{dynamic} = \frac{1}{I} \cdot \frac{dE}{dI} \tag{5.2}$$

The non linear stored energy per unit length, was calculated by OPERA [18]:

$$E = \int \left(\int \underline{H} \cdot d\underline{B} \right) ds \tag{5.3}$$

The plot of the stored energy versus the current is shown in the following Figure 5.7:

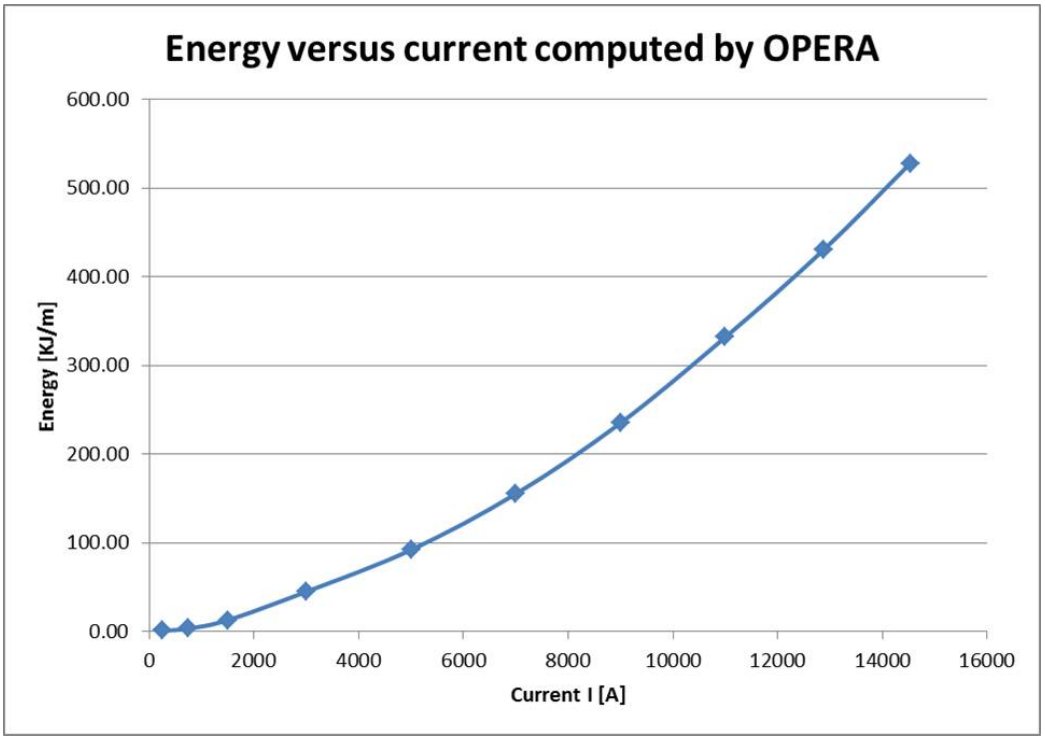

Figure 5.7: Long Quadrupole stored energy per unit length vs, current computed by OPERA

From the value of the stored energy at different currents, reported in Figure 5.7 and Table 5.4, we can obtain from the value of the dynamic inductance per unit length using equation 5.2. Finally by multiplying this value for the magnetic length (l= 3.08 m), we obtain $L_{dynamic}$. This value of stored energy and dynamic inductance are reported in the following Table 5.4 at several currents:

Table 5.4: Values $L_{dynamic}$ computed by OPERA

E [kJ/m]	**I [A]**	**dE [kJ/m]**	**1/I [1/A]**	**dE/dI [kJ/Am]**	**L [H/m]**	**L [mH]**
0.8	250	0.8	$4.00E-03$	$1.60E-03$	$6.40E-03$	19.71
3.3	750	2.48	$1.33E-03$	$4.96E-03$	$6.61E-03$	20.37
12.8	1500	9.52	$6.67E-04$	$9.52E-03$	$6.35E-03$	19.55
44.8	3000	32	$3.33E-04$	$1.60E-02$	$5.33E-03$	16.43
92.0	5000	47.2	$2.00E-04$	$2.36E-02$	$4.72E-03$	14.54
155.2	7000	63.2	$1.43E-04$	$3.16E-02$	$4.51E-03$	13.90
235.2	9000	80	$1.11E-04$	$4.00E-02$	$4.44E-03$	13.69
332.0	11000	96.8	$9.09E-05$	$4.84E-02$	$4.40E-03$	13.55
430.4	12875	98.4	$7.77E-05$	$5.62E-02$	$4.37E-03$	13.45
528.0	14530	97.6	$6.88E-05$	$6.26E-02$	$4.31E-03$	13.26

More details are explained in Appendix 5.2.3.2.

5.2.1.3 Measurements of the inductance at room temperature

Table 5.5, lists measurements of the LQ inductance performed at warm with 1 A at different frequencies. It can be noted that at high frequency the inductance decreases by about 33%.

Table 5.5: Room temperature data

f [Hz]	I [A]	L [mH]
20	1	18.66
120	1	17.18
1000	1	12.50

5.2.1.4 Conclusion of the study of the dynamic inductance

Figure 5.8 shows all LQ inductance values, both measured and computed, at several currents. It should be noted that the experimental values include only data from the 1st area).

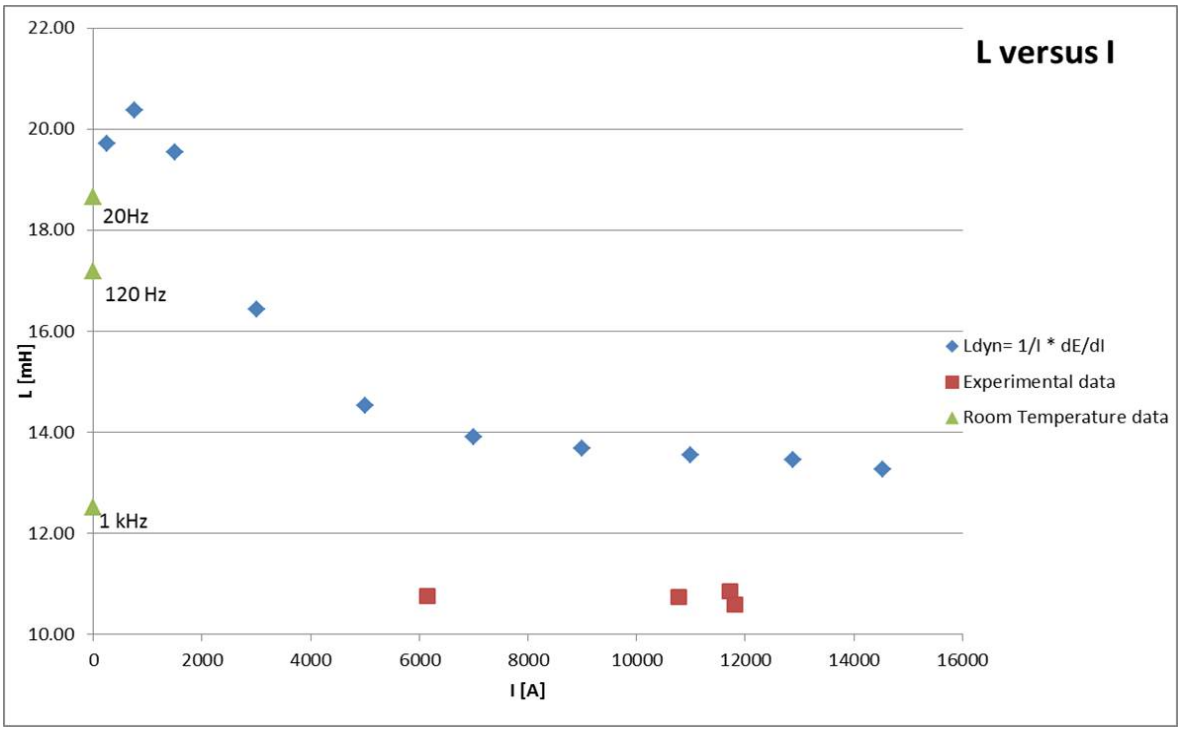

Figure 5.8: $L_{dynamic}$ versus current I

The symbols used in Figure 5.8 represent:

- Blue diamonds: dynamic inductance computed using the stored energy computed by OPERA
- Red squares: experimental values of the inductance computed from the beginning of the current decay (1st *area and the trip*)
- Green triangles: measurements performed at room temperature with 1 A at different frequencies.

In the plot the values computed with OPERA show a significant dependence of the inductance from the current with a decrease of more than 30% at current above 6 kA. The values computed from the current decay show a further decrease of about 30% above 6 kA. We modified QuenchPro in order to accept different values of the inductance depending on the current range. Then we inserted the values shown in Table 5.6.

Table 5.6: Values of the inductance in function of the current put in QuenchPro

Range of current [A]	**Inductance L [mH]**
0-2000	14
2000-5000	12
5000-10000	10.8
10000-13000	10.6

Since we have measured values only at very low current and above 6 kA, the inductance values under 5000 A have been estimated by assuming for the experimental data the same trend of the values computed by OPERA. In any case the values at low current are less important for the quench protection because in this zone there is less heat generation (i.e. small contribution to the MIITs) that at higher currents.

5.2.1.5 Measurements of the effect of the eddy currents on L

The warm measurements presented in Table 5.5 show that eddy currents have a significant effect on the inductance. To explain the effect of the eddy currents on the inductance we can write Kirchoff equation for the circuit:

$$R_d \cdot I_1 + L \cdot \frac{dI_1}{dt} + M \cdot \frac{dI_2}{dt} = 0 \tag{5.4}$$

where I_1 is the current of the magnet and I_2 is the current of the secondary circuit. In our case the second circuit is the copper of the cable or other conductors inside the coil that is coupled to the main circuit given by the coil itself. The eddy currents are the current I_2 circulating in the secondary circuit.

The first term of 5.4 $R_d \cdot I_1$ is > 0,but the second term $L \cdot \frac{dI_1}{dt}$ is < 0 (because dI_1/dt is negative during the current decay in a R-L circuit). The third term $M \cdot \frac{dI_2}{dt}$ is > 0 because is M>0, then $dI_2/dt > 0$ at the beginning of the primary current decay since the eddy are currents growing. Therefore if we study 5.4 in a simplified model neglecting the mutual inductance M and regrouping all inductances in a fictitious self-inductance L_f so that $R_d \cdot I_1 + L_f \cdot \frac{dI_1}{dt} = 0$ then we have

$$L_f = L + M \cdot \frac{\frac{dI_2}{dt}}{\frac{dI_1}{dt}}$$

where $L_f < L$. This explains why our experimental "apparent" self-inductance results lower than the real self- inductance: it is because of the presence of a coupled circuit (or circuits) generating eddy currents.

Since this effect has a significant impact on the current decay during quenches of this magnet, it may be investigating in the future by means of the OPERA code.

5.2.1.6 Comparison of simulated current decay and experimental

After the study of the inductance was completed, we started simulations with QuenchPro of Ramp #1, #2 and #53 (the three Ramps of the 1st area).

We modified QuenchPro to have an inductance changing with current level and to take into account the presence of multiple quench starts, i.e. the 28 heating stations. We also improved the values of the magnetic field used in the simulation by performing a better evaluation of the average field in each coil ($B_{in} = 3.64\,T$ and $B_{out} = 2.62\,T$). We also derived an empirical formula for the dependence of the quench propagation velocity on the ratio $I_{operating}/I_{critic}$. In this way the quench

velocity in QuenchPro is no more an input parameter that needs to be "guessed" or adjustment for each current. The formula is:

$$v_{quench} = 40 \cdot I_{scale}^{3.08}\, m/s$$

where $I_{scale} = I_{operating}/I_{critic}$.

Figures 5.9, 5.10 and 5.11 show the plots comparing the measured current decays (the blue diamonds) and the current decays simulated by the improved QuenchPro (the red squares):

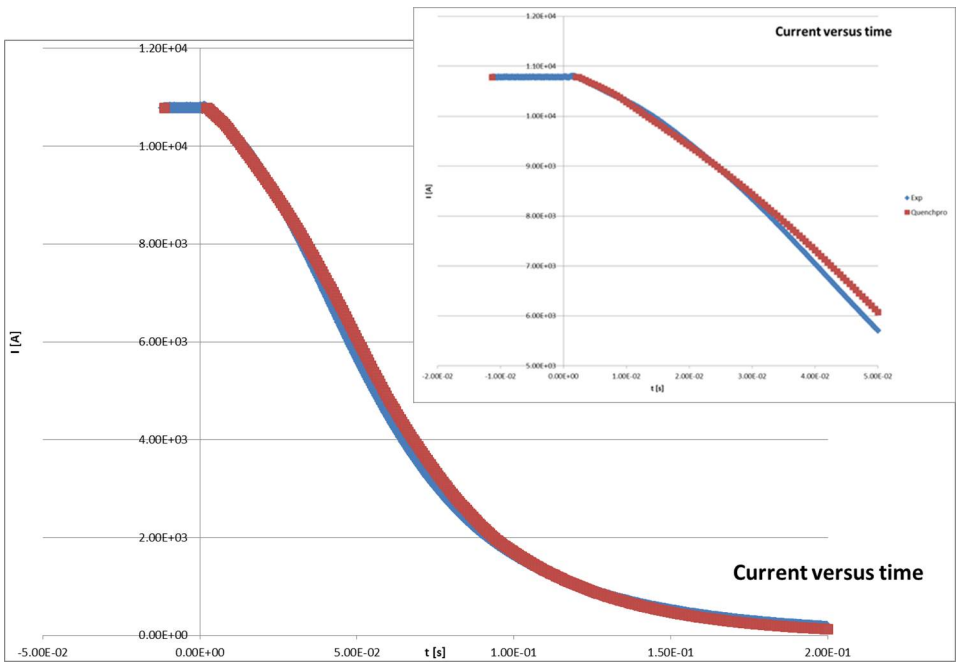

Figure 5.9: Ramp #1

I= 10 782 A with $v_{quench} = 20.01\, m/s$

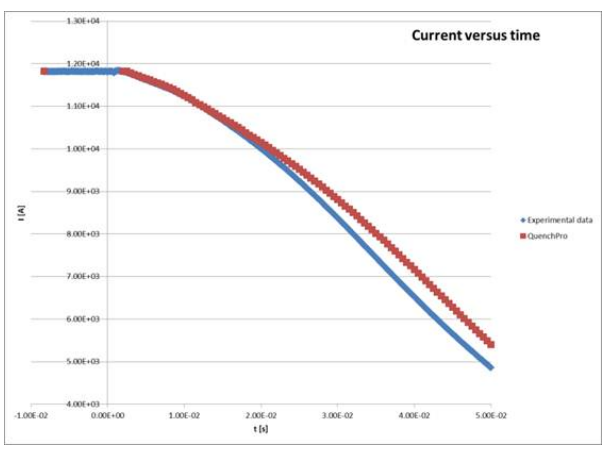

Figure 5.10: Ramp #2

I= 11 818 A with $v_{quench} = 26.55\, m/s$

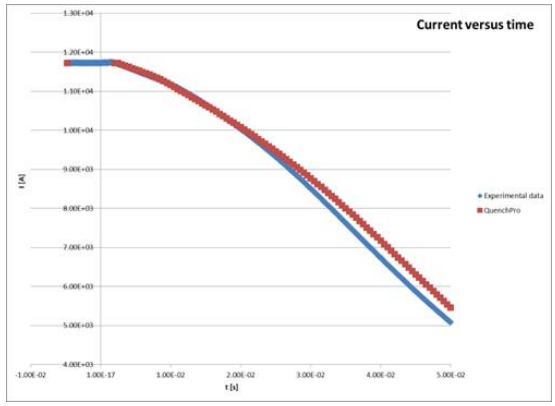

Figure 5.11: Ramp #53

I=11 726 A with $v_{quench} = 25.91\, m/s$

It can be seen that with our improved version, QuenchPro simulates pretty well the shape of the current decay of experimental data. The agreement is almost perfect for the first 3000 A and the difference remain within 3% at half current. At lower currents the difference shrinks again.

5.2.2 Study of the 2nd area

At the beginning of 5.2 we mentioned that in the 2nd area it is maybe present a new phenomenon.

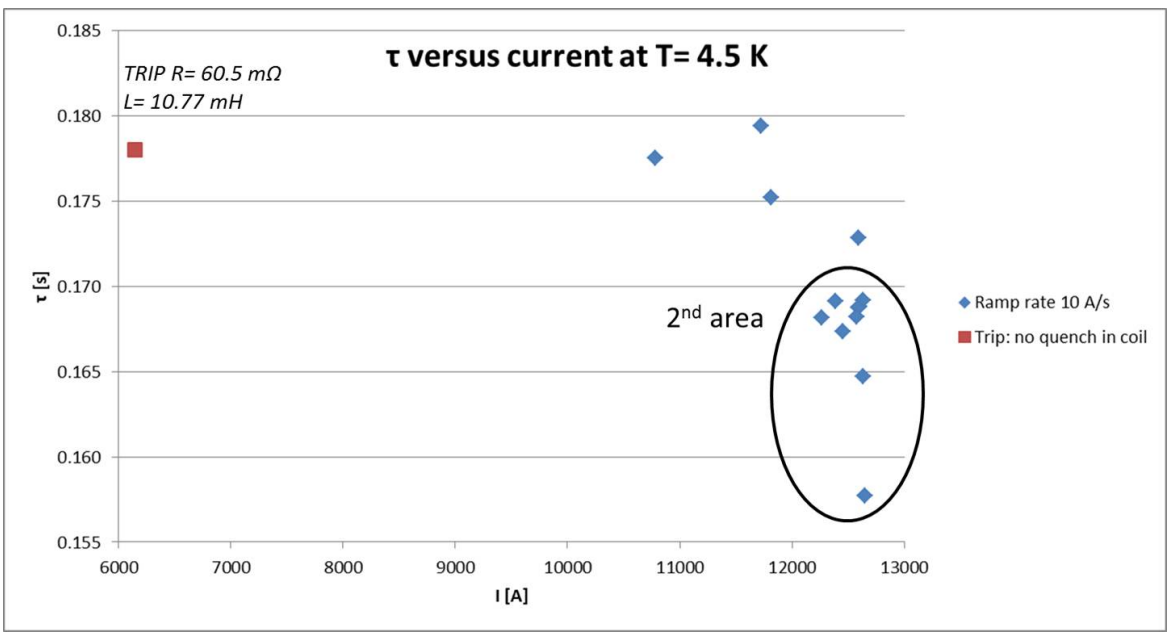

Figure 5.12: τ vs. I

In Figure 5.12 it can be seen that the time constant $\tau = \frac{L}{R}$ decreases considerably with a small increase of current above 12 kA. We do not see a plausible mechanism triggering such sharp inductance decrease. We have therefore explore a possible sharp increase in the effective resistance.

Based on the previous section 5.2.1 we assume a constant inductance (L= 10.60 mH) at high currents. Then from the experimental time constant we obtain the following total resistances of the circuit and the coil resistance: $R_{coil} = R_{tot} - R_{dump}$.

Table 5.7: Resistances data of the 2nd area

Ramp #	**I [A]**	**T [K]**	τ **[s]**	**Coil**	**Segment**	$\mathbf{R_{tot}}$ **[mΩ]**	$\mathbf{R_{coil}}$ **[mΩ]**
33	12390	4.54	0.169	8	b3_b2	62.68	2.18
4	12454	4.54	0.167	6	a11_a12	63.34	2.83
5	12267	4.62	0.168	6	a11_a12	63.04	2.54
26	12602	4.56	0.169	8	b5_b4	62.81	2.31
28	12632	4.56	0.169	8	b5_b4	62.67	2.17
29	12630	4.56	0.165	8	b5_b4	64.35	3.85
52	12652	4.5	0.158	8	b5_b4	67.20	6.70
54	12592	4.55	0.173	8	b5_b4	61.33	0.83
55	12589	4.55	0.169	8	b5_b4	62.82	2.32
56	12577	4.56	0.168	8	b5_b4	63.03	2.53

Usually at the beginning of the quench there is only a small resistance growing around the quench start point. Therefore in order to explain this sharp increase of the resistance we have examined four possible causes:

1. Increase of the effective resistance of the copper stabilized wire generated by a delay in the current diffusion from the Nb_3Sn filaments to the copper. This phenomenon is driven by the magnetic diffusion and its influence increases with higher conductivity and lager size. In our case the current diffusion time can be evaluated by means of the formula [17]: $t_{diffusion} = \frac{l^2 \cdot \mu_0}{\pi^2 \cdot \rho_{Nb_3Sn}}$ where l is the characteristic diffusion length - parameter very similar to the wire diameter. Since $l = 7 \cdot 10^{-4} m$, $\mu_0 = 1.26 \cdot 10^{-6} H/m$ and $\rho_{Nb_3Sn} = 2.40 \cdot 10^{-7} \Omega \cdot m$ at T=20K, we obtain $t_{diffusion} = 2.60 \cdot 10^{-7} s$. This time is completely negligible compared to the time of heat diffusion ($10^{-4} - 10^{-3} s$). Therefore this hypothesis was discarded.

2. A very fast quench propagation around the starting zone. The propagation velocity should be around 20 m/s, however we assume v= 40 m/s to check this hypothesis: $l_{cable\ quenched} = v_{quench} \cdot t \approx 2 \cdot 40 \cdot 0.008 \approx 0.7m$ (taking to account the quench propagates in two directions). Considering a RRR of the Copper of 150, a peak field of 11 T and a cable temperature (just before quench heaters action) of 52 K, the resistance per meter of cable is about $0.21 m\Omega/m$ (see 5.1 for details). Therefore even an improbable double speed in quench propagation cannot generate the $2 - 4m\Omega$ extra resistance. Therefore this hypothesis should be discarded, too.

3. Multiple simultaneous quenches. From the discussion of point 2. we infer that we would need about 10 to 25 simultaneous quench starting points to obtain the measured resistance. Such an occurrence cannot be discarded; nonetheless we consider the probability rather low.

4. Presence of quench back at high currents. In the superconducting cable there is an amount of stabilizer copper in which eddy currents are induces by the ramp down. Referring again to the calculation at the end of 5.1 we know that the cable resistance per meter is $0.21 m\Omega/m$. Then we can obtain the length of quenched cable $l_{cable\ quenched}$ for all ramps (about 10 m based on Table 5.7). Since the total length of the cable in a coil is $l_{cable} = 215m$ we need the quench back mechanism to be able to affect about 5% of the cable, the part that is more sensible to heat diffusion because it is in high field and therefore with a low temperature margin. Another possible cause of "quench back" is the current redistribution in the cable

caused by the quench start. This redistribution can increase the current of some strands above the critical current in points far from the quench onset.

This preliminary analysis suggests the quench back as the most probable mechanism to explain the sharp decrease of the time constant at high currents, through a sudden increase of the coil resistance before the quench heaters had time to heat the coil. An important future development of this work would be to verify the actual presence of quench back by analyzing the voltage tap data in the quench events of the 1st and 2nd area.

5.2.3 Finals comparisons between experimental data, QuenchPro and QLASA

5.2.3.1 QLASA velocities

At the end of this work we decided to use QLASA to have an independent and more precise computation of the quench propagation velocities. In QuenchPro the quench velocity is an input parameter (the formula with the quench velocity as a function of I_{scale} was introduced only at the end of this work), while the code QLASA computes the propagation velocity directly from the general topology of the magnet, the material properties of the conductor and the insulation, the field distribution and the operating current. In the following we show the propagation velocities computed by QLASA for two current ramps.

- Ramp #1

I=10 782 A at T= 4.6 K
Quench initiated in coil 7, segment a7_a8

Table 5.8: Ramp #1 - Quench velocity computed by QLASA

$\mathbf{v_{quench}}$ [m/s]	
12.13	At hot spot in maximum field
10.33	Under the heaters in inner layer
5.57	Under the heaters in outer layer

- Ramp #2

I=11 818 A at T= 4.6 K
Quench initiated in coil 8, segment a7_a8

Table 5.9: Ramp #2 - Quench velocity computed by QLASA

$\mathbf{v_{quench}}$ [m/s]	
14.83	At hot spot in maximum field
12.29	Under the heaters in inner layer
6.25	Under the heaters in outer layer

This velocities are $\sim$ 40% lower compared to the ones computed with the empirical formula presented in 5.2.1.6 and used in QuenchPro at the end of this work.

5.2.3.2 Comparisons

In this section we compare the simulations with the current decay measured at the end of Ramp #2 at I= 11 818 A. Figure 5.13 shows the whole current decay: measured values simulated using QuenchPro and QLASA.

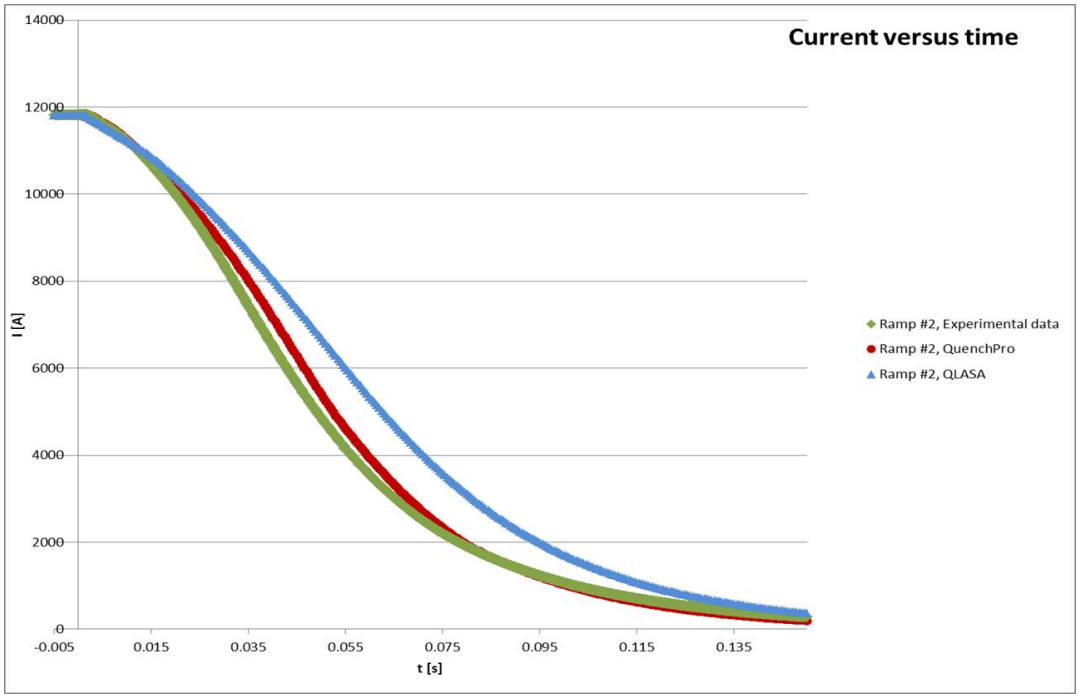

Figure 5.13: Ramp #2

In Fig. 5.13 we plot a zoom of the first 30 ms.

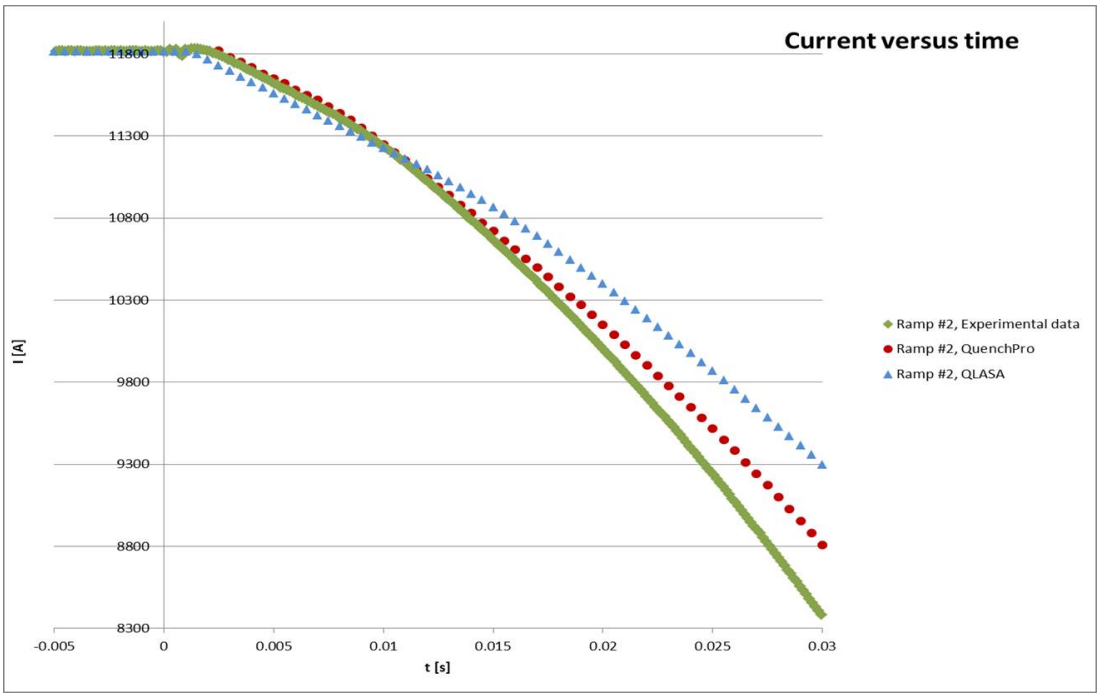

Figure 5.14: Zoom of Ramp #2

From this plot and the previous section we can conclude that QLASA is more conservative because it computes lower quench propagation velocities. This comparisons was performed on many other ramps ans was very useful to understand the dependence of the quench velocity with the current (a functional dependence that is in QLASA but was not present in the original version of QuenchPro). Thanks to this study we have been able to implement the empirical formula in presented in Section 5.2.1.6 ($v_q = v_q\,(I/I_c)$) which is one of the modifications that made QuenchPro simulations significantly more precise.

The modified version of QuenchPro and the other conclusions of this work can now be used for studying the quench protection of other Nb_3Sn magnets with more confidence and more precision.

Conclusions

At the beginning of this work we have find out that there is a serious discrepancy in the current decay during a quench as shown in the experimental data of LQS01b and the QuenchPro simulation. After determining that the inductance was lower than expected, we introduced the concept of dynamic inductance, more suitable for magnets where the iron magnetization changes and the relation between current and field is not anymore linear; this led us to a better understanding of the current decay and to make a good fit. Through these inductance studies we also observed the effect of the eddy currents. After addressing the inductance problem, we were able to implement two improvements of the QuenchPro codes: a better field map over the magnet cross section and a dependence of quench velocity on the current. These modifications allowed us to produce satisfactory simulations in the medium high current quenches. For the very high current quenches, by analyzing a discrepancy between the simulations and the measured time constant of the current decay, we could identify a clear sign of a quench back affecting the coils. Finally the work was completed by adapting the QLASA program for accelerator magnets. Thus, the current decay of the experimental data has been simulated both by QuenchPro and QLASA, which simulations constitute further tools for analysis. This study has evidenced the criticality of protection with respect to some important parameters, such as effective inductance, resistance and quench propagation. For the future it may be interesting to conduct additional quantitative computations of the eddy currents effect and to evaluate more precisely the impact of quench back on the protection; the latter may become useful for magnet protection.

APPENDIX: ENERGY COMPUTED BY OPERA

In this section we will expose how we have computed the energy to obtain the dynamic inductance.

There are two different way of computation of the energy.

The first way is by the following formula 5.5:

$$E = \int \frac{\mathbf{B} \cdot \mathbf{H}}{2} \, ds \tag{5.5}$$

which is the stored energy/unit length which is valid only in case of linear relation between B and H.

The second possibility is by 5.6:

$$E = \int \left(\int \mathbf{H} \cdot \mathrm{d}\mathbf{B} \right) ds \tag{5.6}$$

which is the non linear stored energy/unit length, i.e. the formulation which is valid in the general case (to be used when magnetization is variable with current).

$B = \mu H$ and in 5.5 μ is a constant. While in 5.6 μ is not a constant in function of the field (or of current).

In the Table 5.10 we have:

Table 5.10: Values of Energy and Nlenergy in function of current

I [A]	**Energy [kJ/m]**	**Nlenergy [kJ/m]**
100	0.0328	0.0328
500	0.8	0.8
1000	3.28	3.28
2000	12.8	12.8
4000	48	44.8
6000	100	92
8000	169.6	155.2
10000	256	235.2
12000	360	332
13750	464.8	430.4
15310	569.6	528

The plot is reported in Figure 5.15.

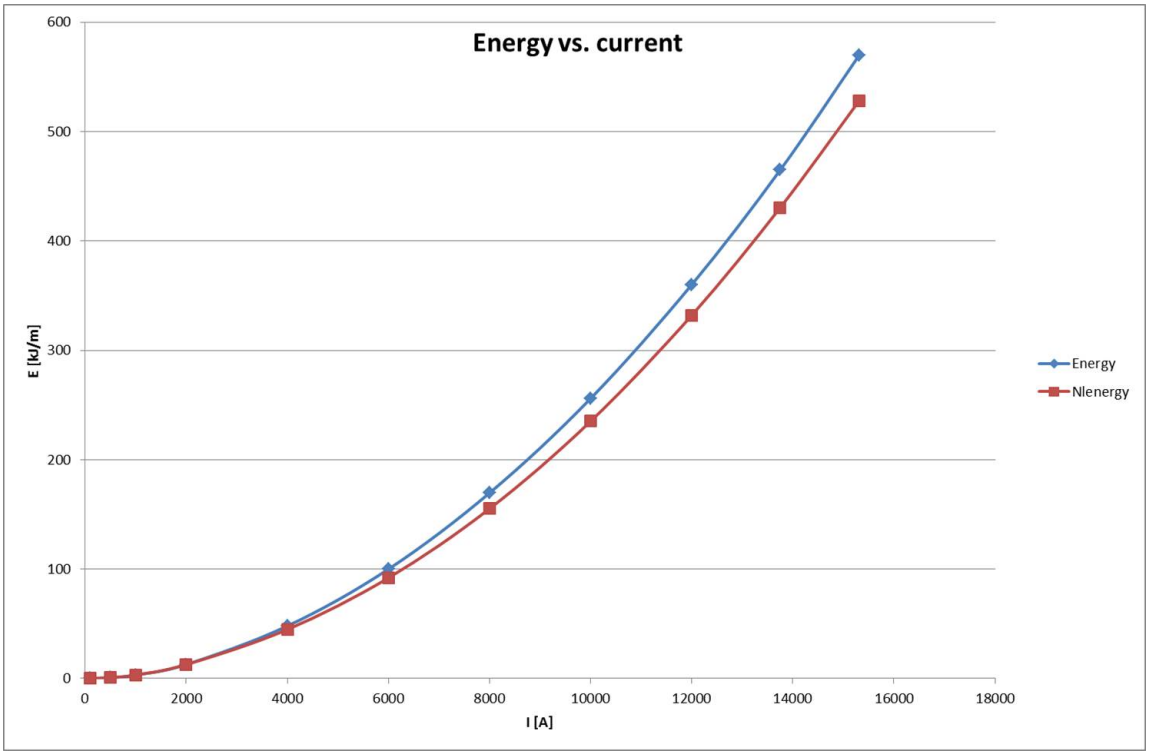

Figure 5.15: Energy and Nlenergy versus current

Clearly the formulation of the linear formula is not sufficient in our case, therefore we have used the expression given by Equation 5.6.

Acknowledgments

This work was possible thanks the courtesy of the Head of the Technical Division, **Giorgio Apollinari**, to whom I am grateful for the opportunity of collaboration.

A sincere acknowledgment to my supervisor **Giorgio Ambrosio** who is a very good example of researcher and that has shown a great patient and attention during all this period. Thanks for the joy and the constancy you have in your work, you are an example to me. Grazie!

Thanks to my University professor **Massimo Sorbi** to accept to be my supervisor, and thanks for the courtesy and for the help in particular during some work difficult moments at Fermilab and thanks for the review of the thesis.

Thanks to **Guram Chlachidze** for the kindness, during all my permanence. Special thanks for the tour to the Test Facility and the afternoons during the magnet tests. It was very instructive and interesting. Also many thanks are due for helping the redaction of the thesis and providing useful materials.

Thanks also to the other colleagues of the Fermilab Magnet group: **Michael A. Tartaglia**, **Riuji Yamada**, **Alexander Zlobin**, and all the group of the Technical Division for the discussions and support. Many thanks also for the useful discussion to **Helene Felice** and **Tiina Salmi** of LBNL.

Bibliography

[1] M. Wilson, "Superconducting magnets", Oxford UK: Clarendon Press, 1983

[2] L. Rossi, "Superconducting Magnets", CERN Academic Training, 15-18 May 2000

[3] Fermi National Accelerator, Batavia (Illinois), USA, http://www.fnal.gov/

[4] The Large Hadron Collider, CERN, http://lhc.web.cern.ch/lhc/

[5] International Linear Collider, http://www.linearcollider.org/

[6] A. Devred, "Practical low-temperature superconductors for electromagnets", CERN - 2004 - 006, 2006

[7] K.-H. Mess, P. Schmuser, S. Wolff, "Superconducting accelerator magnets", Singapore: World Scientific, 1996

[8] A. Godeke, "Performance boundaries in Nb_3Sn superconductors", PhD thesis, 2005

[9] D. Dietderich, "Development of High Current Nb_3Sn Rutherford Cables for NED and LARP", WAMSDO 2008, CERN, Geneva, 2008

[10] G. Ambrosio et al., "Long Quadrupole design report", Version 22, LARP_note_2008

[11] G. Ambrosio, et al., "LARP LQS01b Magnet Test Summary", FNAL TD-10-023. Available: http://tdserver1.fnal.gov/tdlibry/TD-Notes/

[12] P. Bauer et al., "Concept for a Quench Calculation Program for the Analysis of Quench Protection Systems for Superconducting High Field Magnets", FNAL TD-00-027. Available: http://www-td.fnal.gov/info/td_library.html

[13] L. Rossi, M. Sorbi, "QLASA: a computer code for quench simulation in adiabatic multicoil superconducting windings", INFN/TC-04/13, 6 Luglio 2004, Rev.1, Available: http://www.lnf.infn.it/sis/preprint/

[14] Photos by the courtesy of G. Chlachidze, FNAL

[15] M.J. Lamm, et al., "A new facility to test superconducting accelerator magnets", FNAL TD-97-072, Available: http://tdserver1.fnal.gov/tdlibry/TD-Notes/

[16] G. Manfreda, L. Rossi, M. Sorbi, MATPRO-Upgraded version 2012: A computer library of materials property at cryogenic temperature, Report INFN -12-04/MI, April 20, 2012

[17] M. Pellegatta, "Studies and measurement on the normal zone propagation following a quench in ATLAS/B0 superconducting magnets", Graduation thesis, PACS code 85.25.S Milan University, Physics Departement, 19, 2002.

[18] OPERA-3D, Finite elements code, Vector Fields Limited, Oxford UK.